Z-SOURCE INVERTER BASED BOOSTED VOLTAGE FLUX-WEAKENING CONTROL OF SPMSM

DISSERTATION/THESIS

SUBMITTED IN PARTIAL FULFILLMENT OF THE REQUIREMENTS FOR THE AWARD OF THE DEGREE
OF

MASTER OF
TECHNOLOGY IN
POWER ELECTRONICS AND SYSTEMS

Submitted by:

ABHISHEK DALAL

2K21/PES/04

Under the supervision of

Prof. Mini Sreejeth
(Professor, EED, DTU)

DEPARTMENT OF ELECTRICAL ENGINEERING

DELHI TECHNOLOGICAL UNIVERSITY

(Formerly Delhi College of Engineering)

Bawana Road, Delhi-110042

2023

M.Tech (Power Electronics and Systems) Abhishek Dalal 2023

DEPARTMENT OF ELECTRICAL ENGINEERING

DELHI TECHNOLOGICAL UNIVERSITY

DECLARATION

I, Abhishek Dalal, Roll No. 2K20/PES/04 student of M.Tech (Power Electronics and Systems), hereby declare that the project Dissertation titled **"*Z-Source Inverter Based Boosted Voltage Flux-Weakening Control of SPMSM*"** which is submitted by me to the Department of Electrical Engineering Department, Delhi Technological University, Delhi in partial fulfilment of the requirement for the award of the degree of Master of Technology, is original work and not previously used for the award of any Degree.

Abhishek Dalal

2K21/PES/04

DEPARTMENT OF ELECTRICAL ENGINEERING

DELHI TECHNOLOGICAL UNIVERSITY

CERTIFICATE

This is to certify that the dissertation entitled ***"Z-Source Inverter Based Boosted Voltage Flux-Weakening Control of SPMSM***" being submitted by Abhishek Dalal (2K21/PES/04) in partial fulfillment of the requirements for the award of Master of Technology degree in "ELECTRICAL ENGINEERING" with specialization of "POWER ELECTRONICS & SYSTEMS" at the Delhi Technological University is an authentic work carried out by him under my supervision and guidance.

To the best of my knowledge, the matter embodied in the thesis has not been submitted to any other University/ Institute for the award of any degree or diploma.

Prof. Mini Sreejeth

Professor

Electrical Engineering Department

Delhi Technological University

Date: 31-05-2022

Place: Delhi

ACKNOWLEDGEMENT

I take this opportunity to express my deepest gratitude and appreciation to my project supervisor **Prof. Mini Sreejeth**, Professor, Delhi Technological university and Head of Department **Prof. Pragati Kumar**, Delhi Technological university for their everlasting support.

I am thankful to her for suggesting the various aspects of the problem and project, rendering help during fabrication of work and rendering encouragement during the various phases of work.

I would like to thank my friends and all those who have helped me and encouraged me in completion of my dissertation in time.

Finally, I thank my parents for their moral support and confidence which they showed in me to pursue M. Tech at the advanced stage of my academic career.

Abhishek Dalal

ABSTRACT

Z-SOURCE INVERTER BASED BOOSTED VOLTAGE FLUX-WEAKENING CONTROL OF SPMSM

This thesis gives a brief analysis of field-oriented control strategy for flux-weakening and maximum torque per ampere (MTPA) operation of permanent magnet synchronous motor (PMSM). Features such as higher efficiency, smaller size, faster dynamic response and large torque-to-inertia ratio makes the application of PMSM suitable for the electric vehicle (EV). However, because of permanent magnet on rotor, i.e., constant flux, permanent magnet (PM) motors have small constant power speed range (CPSR). This drawback limits the application of PMSM in EV's where wide speed operation, above base speed, is required. The high-speed operation under constant power zone can be extended either by (1) increasing the output voltage of drive or (2) by using flux-weakening control methods. However, the dc bus limits the output voltage of a conventional drive. Further, the high-speed operation, i.e., above base speed is limited by the voltage constraint from the drive side which is the maximum voltage a conventional inverter can output. Ultimately, this is in-turn depends on dc bus voltage rating and usually application like EVs has limited dc bus normally rated for 200 to 600 volts. That's why in this thesis an advanced flux-weakening algorithm is introduced aimed for providing wide constant power operation namely, boosted voltage flux-weakening (BVFW), based on the Z-source inverter (ZSI). A ZSI has voltage boosting abilities and is immune to shoot-through issues. This flux-weakening strategy overcomes the voltage constraint in electrical drives fed from a conventional inverter by utilizing the voltage boosting ability of Z-source Inverter (ZSI) for a wide speed operation, i.e., above base speed. In comparison to other flux weakening control strategies, this method can provide wide constant power speed range (CPSR) with higher torque generation. Moreover, the maximum boost control method is also been discussed for controlling the shoot-through state of ZSI. In order to validate the feasibility and merits of the ZSI based flux-weakening algorithm, a SPMSM drive with MTPA and BVFW controls based on ZSI has been simulated in MATLAB/SIMULINK and its performance is compared with other conventional flux-weakening strategies.

TABLE OF CONTENTS

LIST OF FIGURES

LIST OF TABLES

NOMENCLATURE

SPMSM	Surface Permanent Magnet Synchronous Motor
PMSM	Permanent Magnet Synchronous Motor
ZSI	Z-Source Inverter
b-EMF	Back-Electromotive Force
CPSR	Constant Power Speed Range
EV	Electric Vehicle
PM	Permanent Magnet
FOC	Field Oriented Control
DTC	Direct Torque Control
MTPA	Maximum Torque Per Ampere
CVCP	Constant Voltage Constant Power
VCLFW	Voltage and Current Limited Flux-Weakening
BVFW	Boosted Voltage Flux-Weakening
SVPWM	Space Vector Pulse Width Modulation
SPWM	Sinusoidal Pulse Width Modulation
PWM	Pulse Width Modulation

CHAPTER 1

INTRODUCTION

1.1 BACKGROUND

In past few years, research on permanent magnet synchronous motor (PMSM) has drawn a lot of attention in many industrial applications, especially in traction application due to its attractive performance i.e., large torque-to-inertia ratio, smaller size, higher efficiency, high-power density, faster dynamic response and decrease in cost of permanent-magnets [1-2]. In electric vehicles (EV), PMSM drives generally requires large torque-to-inertia ratio for below base speed operation and high efficiency along with wide constant power speed range (CPSR) [3-4]. In recent studies, the research on field-oriented control of PMSM drives aimed for the above-mentioned application has becoming increasingly common [5-10].

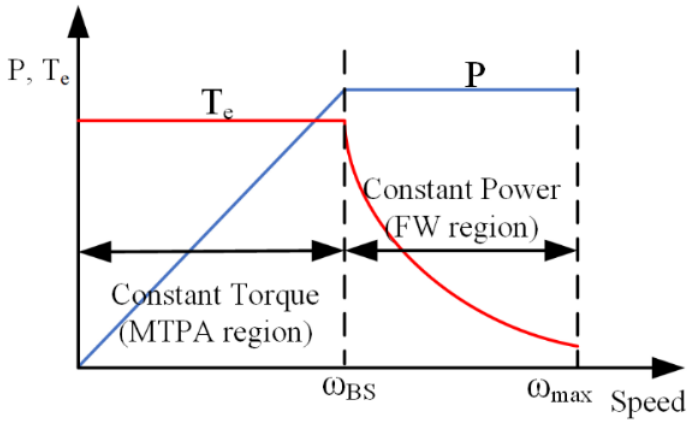

Fig.1.1: Typical Torque/Power vs. Speed curve of PMSM.

Moreover, recently various control techniques has been published in literature aimed for achieving efficient performance of drive under varying condition. One such control technique is maximum torque per ampere control (MTPA) [11], extensively used in industrial applications due to its effective utilisation of dc bus, maximum torque generation, and minimisation of copper losses. For wide speed operation in PMSM drives, i.e., above base speed, flux-weakening (FW) control is required which extends the speed range of motor by decreasing the air-gap flux [12]. In application focused on electric vehicles, PMSM drives are intended to deliver constant torque for below base speed operation while for above base speed operation, torque gradually reduces upto maximum

speed. Therefore, PMSM drives are operated with flux-weakening control in constant power zone and MTPA control in constant torque zone as shown in fig. 1.1 [13].

Hence, it is of significant importance to improve the flux-weakening capability of PMSM drives. The subsequent sections describe the flux-weakening control of PMSM in traction application, and an advanced control method to enhance the constant power speed range performance by utilising the voltage boosting capabilities of z-source inverter.

1.2 LITERATURE REVIEW

1.2.1 Control Strategies for PMSM

PMSMs are brushless motors that employs stationary phase coil and rotating permanent magnet. A 3-phase PMSM's stator has a construction that is substantially identical to that of a 3-phase synchronous machine or a 3-phase induction machine. A rotating magneto-motive force (MMF) with a circular trajectory in d-q frame is generated in the air-gap by these phase currents. Although, the Permanent Magnets can be placed either inside or on the rotor structure to form interior permanent magnets or surface-mounted permanent magnets in the rotors of PMSM.

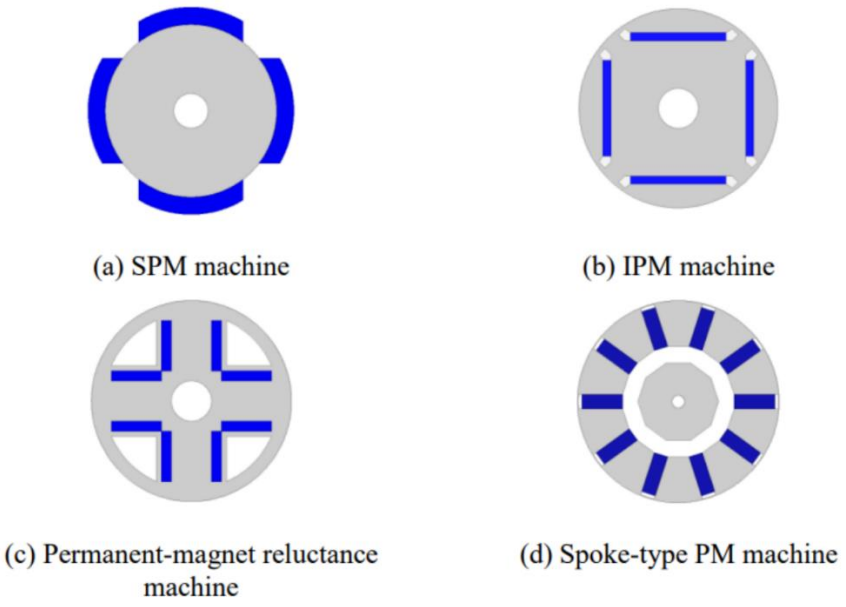

Fig.1.2: Rotor configurations for permanent magnet machines.

As shown in fig. 1.2, there are four common permanent magnet configurations for rotor in PMSMs. These includes, (a) interior-mounted, (b)

surface-mounted, (c) spoke-type and (d) reluctance-type [14]. The saliency ratio of the permanent magnet's inductance (L_d/L_q) in the various rotor configurations has a major impact on the operating speed range. However, the application decides which rotor layout is viable. In this research work, the discussion is focused on surface-mounted (SPMs), which are extensively employed in industrial application.

In general, scalar and vector control are the two main types of motor control techniques, widely used in controlling of AC machines and are applicable for control of PMSM also [15]. Moreover, there are particularly three primary control strategies in scalar and vector control methods [16]:

• Volts/hertz control

• Direct torque control (DTC)

• Field-oriented control (FOC)

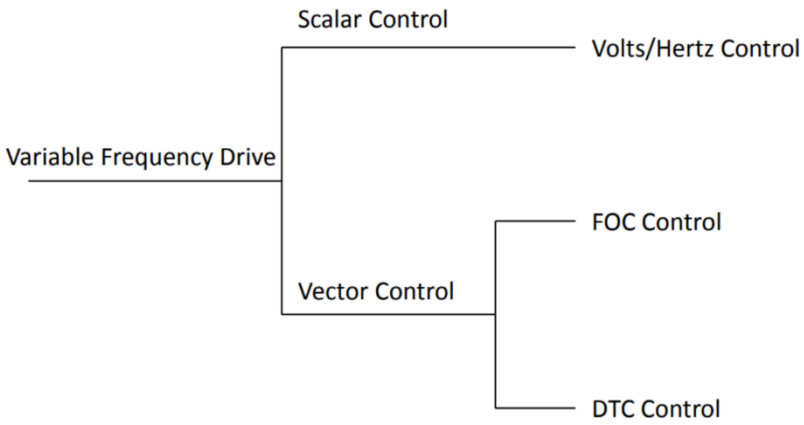

Fig.1.3: Motor control classification.

Fig. 1.3 shows the categorization of different motor control techniques. The scalar control technique is also referred as volt/hertz (V/f) control, used for rather easier applications like fans and pumps. A constant air-gap flux is produced, when PMSM are excited by constant V/f ratio. The V/f control is a very popular and economical technique that is frequently used in industrial applications. Despite that due to its relatively poor dynamic response is not very effective because rather than controlling the magnitude and phase of current, this technique instead controls the frequency and magnitude of voltage [15]. On the other hand, vector control techniques, namely DTC and FOC, are rather difficult but they provide high accuracy with relatively faster dynamic performance. The basic concept for field-oriented control is to transform the time-varying

three-phase currents into equivalent synchronously rotating d-q frame where flux torque controlling components are decoupled and controlled independently [17]. Whereas, in direct torque control the space vector modulation technique is used for direct control of the torque and stator flux in accordance with the variation between the reference and estimated values for flux and torque. The direct torque control is less immune to the variation in stator resistance but can provide fast dynamic performance in comparison to the field-oriented control. Due to the comparative advantages of V/f, DTC, and FOC, it is challenging to decide which method should be preferred. Finally, in order to decide which control technique has to be used is based on the performance parameters required by an application.

Based on FOC, various control techniques are available to control the PMSM aimed for different control objective are listed below:

• Unity power factor control [18]

• Optimum efficiency control [19]

• MTPA control [20]

• Flux-weakening control [20]

MTPA and flux-weakening controls are widely used in electrical drives as compared to unity power factor and optimal efficiency controls. They are opted because of their merits such as extended speed range operation in constant power zone and maximum torque generation with minimum copper losses in constant torque zone offered by the flux-weakening control and MTPA control respectively.

The control of PM motors for EV applications has attracted a lot of interest in recent publications due to their efficient and high power-density performance [6-21], permanent magnet motors emerged as the best alternative to internal combustion engines. In traction and other industrial application, the ability to operate with high efficiency over an extended speed range is required. That's why most of the PMSM drives in practical applications are controlled with MTPA control in below base speed operation and flux-weakening control for above base speed operation [22-24].

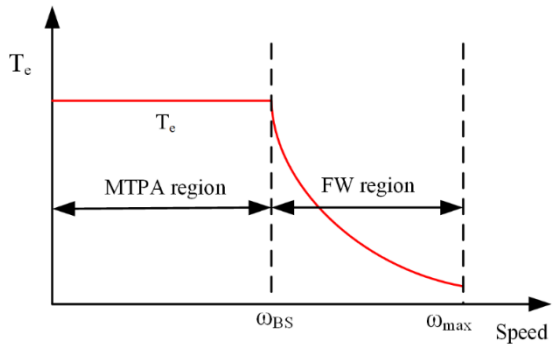

Fig.1.4: Ideal torque vs. speed curve of PMSM.

Fig. 1.4 shows that in constant torque zone, by implementing the MTPA control maximum torque generation is achieved. while in constant power zone, flux-weakening control is implemented in which an opposing field is produced which reduces the field due to permanent magnets by allowing the stator currents to re-orient their position [20]. Therefore, the main principle of flux-weakening operation is to reduce the resultant air-gap flux. In rotating machines, the operating speed is inversely proportional to air-gap flux. Thus, weakening the air-gap flux results in extended speed range operation.

The concept for MTPA operation is that for maximum torque production torque angle has to be controlled, angle between positive stator d-axis direction and stator current phasor in synchronously rotating frame fixed to rotor. To be specific, for any torque level there exists an optimal combination of q-axis and d-axis current which produces minimum phase current [20]. This leads to the reduced copper losses and hence maximizes the motor-drive efficiency.

As rotor field of a PMSM is a set quantity that depends on material and configuration of the permanent magnets [12], that's why the word "flux-weakening" is preferred over the less specific "field-weakening". To be more precise, field-weakening can only be used on motors where field is controlled by the currents. Therefore, the aim of flux-weakening operation is to extend the operating speed range of motor in constant torque zone by reducing the output torque level. There are two main reason that serves such purpose. It is the sole approach to increase the speed range further when voltage and currents are constrained. Secondly, it has been noted in numerous publication, particularly those focused on electric vehicles, that the motor speed is inversely proportional to the load torque.

The concept for flux-weakening operation in PMSM drives is that, d-axis in stator d-q reference frame is oriented in the direction of rotor flux. Therefore, on supplying a negative (demagnetizing) d-axis current to stator establishes a demagnetizing MMF which will negate the MMF due to permanent magnets placed on the rotor. This results in the weakening of resultant air-gap flux. As air-gap flux and output torque are directly proportional to each other, therefore at the cost of reduced output torque a wide speed range can be attained by implementing the flux-weakening control.

Research on flux-weakening control technique is discussed in numerous literatures [25-27]. Several flux-weakening strategies has been published recently, even though their goals are similar. The flux-weakening technique employed for control of AC motor drives was originally presented in [23]. The flux-weakening control is achieved by modifying the feed forward torque control in [12]. In order to maximize the dc bus utilisation, a six-step voltage control is discussed in [28]. An advanced feed-forward decoupled control for current regulator with voltage compensation is introduced in [24]. The ease in execution as well as ability to adjust to variations in machine variables are two main merits of this method.

One significant limitation of all conventional flux-weakening techniques is that back-EMF is directly proportional to the motor speed thus its magnitude should be observed carefully. In electric vehicle applications, dc bus size is limited which in turn limits the maximum output voltage of inverter. Therefore, the instant when magnitude of back-EMF becomes more than the maximum output voltage that an inverter can output, further increase in operating speed cannot be achieved. Hence, the operating speed range of PMSM drives fed from a conventional inverter is constrained by the limitation set from the drive's side. In subsequent section in order to overcome the drawbacks of conventional drives an advanced Z-source inverter-based flux-weakening strategy is introduced which is aimed to extend the constant power speed range and enhance the flux-weakening performance.

1.2.2 Z-Source Inverter (ZSI)

All flux-weakening strategies has two constraints specifically the voltage limitation and current limitation. Generally, the current limitation is decided from the thermal ratings of motor whereas the drive side decides the voltage limitation which has

limited dc bus voltage. In electric vehicles, dc bus voltage typically ranges from 300 to 600 V [29], while for 3-phase industrial drives dc bus is rated for 320 V. Fig. 1.5 shows that for a fixed dc bus voltage, the maximum output line voltage for the conventional 3-phase six-step inverter operating in 180 conduction mode is 78% of dc bus voltage [30]. In sinusoidal pulse width modulation (SPWM) inverter, it is 61.2% of dc bus voltage [30]. While, in space vector pulse width modulation (SVPWM) inverter it is 70.7% [27]. Therefore, it is clear that the output voltage of conventional inverter irrespective of any modulation technique is limited by the voltage constraints.

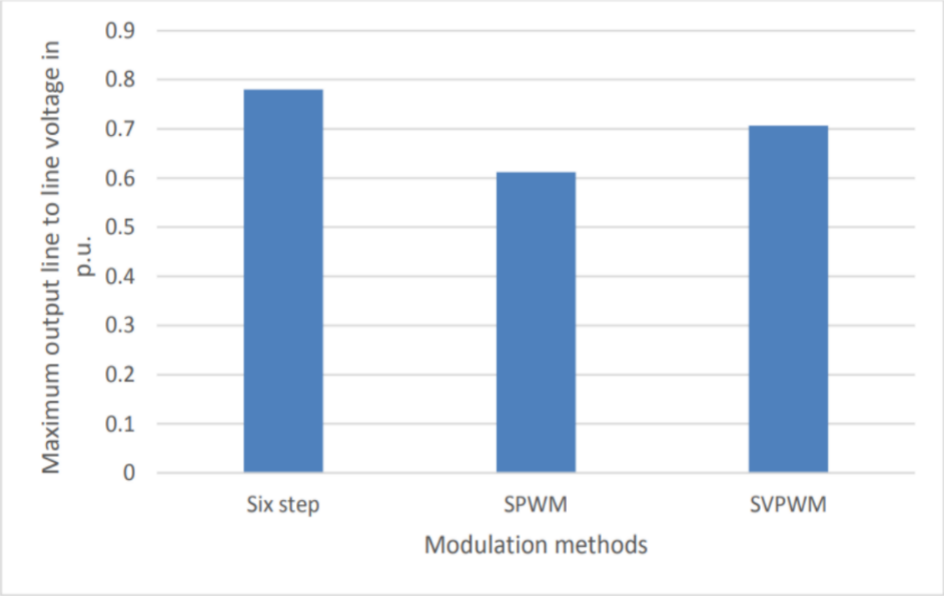

Fig.1.5: Maximum output voltage of 3-phase full-bridge inverters.

There are many different kinds of topologies that can raise the drive's output voltage rather than a dc-dc boost converter. Emerging boost inverters, such as the newly introduced ZSI [31] and its modified topology, quasi-Z-source inverter (q-ZSI) [32], are ideal to supply various application, which includes fuel cell and hybrid vehicles also [33]. Fig. 1.7 shows that an unique impedance network similar to ZSI can replace the dc-dc boost stage. One valuable advantage of ZSI and q-ZSI is that these single-state converters have the ability to buck and boost the dc bus voltage, which eliminates the necessity of using a dc-dc boost converter [34]. This merit could be utilized to remove the constraint of output voltage in drives fed from conventional inverters. Additionally, the ZSI has fault-tolerant abilities against voltage sags and shoot-through fault. That's why, motor drives involving the ZSI have drawn significant attraction in recent publications [35-36].

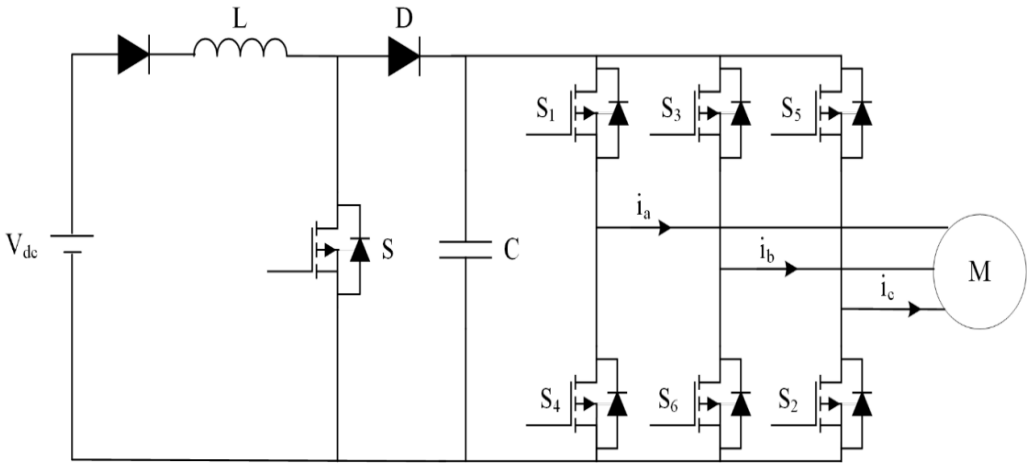

Fig.1.6: Two-stage motor drive comprising DC-DC boost converter and 3-phase inverter.

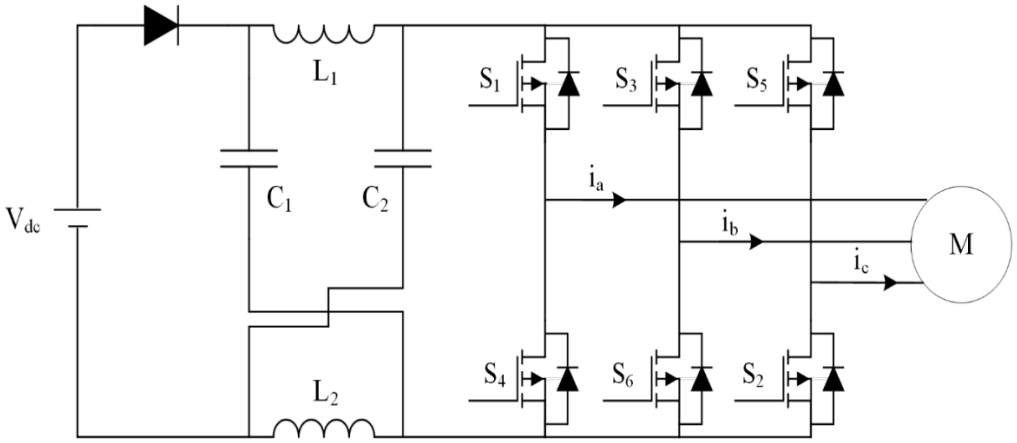

Fig.1.7: Single-stage motor drive using Z-source inverter.

There exist various classic converters, like Z-source matrix inverter [37] and Z-source multilevel inverter [38], that can give additional benefits by employing the impedance network of ZSI. Furthermore, recently in many literatures enhanced ZSI, i.e., switched inductor ZSI [39] and modified ZSI [40], to achieve additional benefits are also introduced. For simplicity purpose, the entire focus is concentrated upon the original ZSI and a detailed analysis given in chapter-3.

A ZSI has two control variables, namely, the modulation index and shoot through states, in comparison to a conventional SPWM inverter which has modulation index as the only control variable. There are three popular control method for ZSI:

- Maximum constant boost method [41]
- Maximum boost method [42]

- Simple boost method [32]

In ZSI control strategies, advance techniques such as SVPWM is also available [43] but the main difference among these strategies exists in their voltage stress across switches, harmonic distortion and voltage boosting capabilities.

In literatures survey, it is found that only few publications have examined the implementation of ZSI for flux-weakening operation in electric vehicles application and very limited research is done on the control strategies of ZSI during flux-weakening operation. Thus, an appropriate control strategy for ZSI, aimed to extend the constant power speed range and enhance the flux-weakening performance, should be developed for supporting the boosted voltage flux-weakening control.

1.3 THESIS ORGANIZATION AND CONTRIBUTION

This work presents an advance flux-weakening strategy for SPMSM. The main advantage of the above-mentioned strategy is that it overcomes the voltage constraint from drive's side during flux-weakening operation by employing the Z-source inverter. In order to validate the viability and merits of the discussed control algorithm, the SPMSM drive is simulated in MATLAB/Simulink environment and compared with other flux-weakening algorithms. The theoretical analysis and simulation results shows that the discussed flux-weakening algorithm can significantly enhance the constant power speed range and delivers higher torque while maintaining the output power constant.

The thesis organization is as follows:

Chapter-1: The literature survey of PMSM, flux-weakening techniques and ZSI is presented.

Chapter-2: The conventional flux-weakening strategies are discussed.

Chapter-3: Briefly discusses the operating principle and control methods of ZSI.

Chapter-4: Demonstrate the ZSI based boosted voltage flux-weakening control of SPMSM drive.

Chapter-5: summarises the conclusion and accomplishment of this work.

CHAPTER 2

CONTROL OF PERMANENT MAGNET SYNCHRONOUS MOTOR

Control strategies are essential for maximizing the efficiency and torque-power capabilities of PMSM over a wide speed range. In the following sections a detailed analysis of flux-weakening and maximum torque per ampere (MTPA) control techniques is presented for SPMSM motor. The mathematical model of PMSM is first developed before analysing the control strategies.

2.1 INTRODUCTION

It is observed that PMSM are gaining popularity for the vast number of applications in industry, ranging from high-performance drives i.e., servo tools to relatively simple application such as fans and pumps [16]. PMSM drives for the above-mentioned application are usually aimed for wide speed range with maximum efficiency.

In traction application, generally drive's speed is inversely proportional to the load torque. Also, at low-speed operations load torque demands are high that's why MTPA control is preferable for maximum torque generation. Both the induction motor as well as PMSM are usually controlled using MTPA control in below base speed operation. In traction application, i.e., EV, at high-speeds torque requirement isn't as high as in low-speed operation. However, the wide speed range is more preferable objective for above-mentioned application for high-speed operation. That's why flux-weakening control becomes more desirable and crucial for above base speed operation.

Generally, high speed operation is feasible with both SPMSM, that has surface mounted magnets which offers no saliency $(L_d = L_q)$, and IPMSM, that has interior mounted magnets which offers high saliency $(L_q > L_d)$ [44]. Due to high inductance value in IPMSM as compared to SPMSM, IPMSM has an advantage of relative low values of demagnetizing currents in flux-weakening operation [45]. Additionally, IPMSM can withstand high centrifugal forces due to interior mounted magnets in rotor, this leads to a robust mechanical structure. Although, the control of IPMSM is difficult because of its saliency and involves complex computation. Therefore,

SPMSM are widely used in vast range of applications including in EVs for its simple control process.

2.2 MATHEMATICAL MODEL OF PMSM

Based on farad's law, the electrical circuit equation of PMSM in terms of phase variable is given by:

$$V_a = R_s I_a + \frac{d\lambda_a}{dt} \tag{2.1}$$

$$V_b = R_s I_b + \frac{d\lambda_b}{dt} \tag{2.2}$$

$$V_c = R_s I_c + \frac{d\lambda_c}{dt} \tag{2.3}$$

Here, R_s (V_a, V_b, V_c) and (I_a, I_b, I_c) refers to the per-phase resistance, phase currents and phase voltages respectively.

The flux linkage equations for the three-phases can be written as follows [26]:

$$\lambda_a = L_{aa} I_a + L_{ab} I_b + L_{ac} I_c + \lambda_{ma} \tag{2.4}$$

$$\lambda_b = L_{ab} I_a + L_{bb} I_b + L_{bc} I_c + \lambda_{mb} \tag{2.5}$$

$$\lambda_c = L_{ca} I_a + L_{cb} I_b + L_{cc} I_c + \lambda_{mc} \tag{2.6}$$

Here, (L_{aa}, L_{bb}, L_{cc}) represents the self-inductances and $(L_{ab}, L_{bc}, L_{ca} \cdots)$ represents the phase-phase mutual inductance. Whereas, $(\lambda_{ma}, \lambda_{mb}, \lambda_{mc})$ refers to the induced flux linkage in stator phases by permanent magnets.

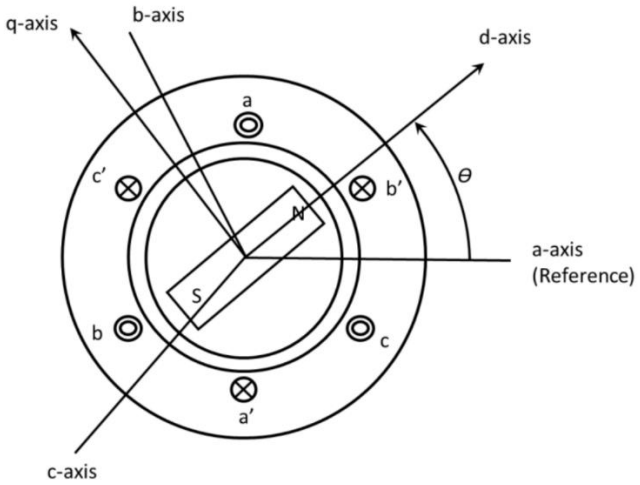

Fig.2.1: d-q coordinate frame of PMSM.

From equations (2.4)-(2.6), It is observed that inductances are function of rotor position which is the angle between positive stator d-axis direction and stator current phasor in synchronously rotating frame fixed to rotor as shown in fig. 2.1. Therefore, the stator winding's flux linkage induced by permanent magnets can be rewritten in the following way:

$$\lambda_{ma} = \lambda_{pm} \cos \theta \tag{2.7}$$

$$\lambda_{mb} = \lambda_{pm} \cos\left(\theta - \frac{2\pi}{3}\right) \tag{2.8}$$

$$\lambda_{mc} = \lambda_{pm} \cos\left(\theta - \frac{4\pi}{3}\right) \tag{2.9}$$

Here, λ_{pm} is the amplitude of permanent magnet flux linkage and rotor angle (θ) is obtained by integrating the electrical speed of motor (ω_e):

$$\theta = \int \omega_e dt + \theta_0 \tag{2.10}$$

Where, θ_0 is the initial rotor position.

In general, the PMSM is similar to the transformer with a rotating secondary winding and the coupling coefficient between rotor and stator windings changes continuously with respect to the rotor angle [20]. The PMSM can be modelled in synchronously rotating 'abc' reference frame which has continuous time-varying inductance values. Although, due to time-varying inductances such a model becomes quite complex. In 1929, Robert H. Park introduced an entirely novel approach known as Two-reaction theory or d-q Park transformation, intended to resolve the challenges associated with the time-varying inductance values. By using the Park transformation, the 3-phase time varying-quantities are transformed into equivalent dc quantities in synchronously rotating d-q reference frame. The generalized form of Park transformation is given by:

Let U and T represents the 3-phase time-varying electrical quantities i.e., currents, voltages, or flux-linkages and Park transformation matrix respectively.

$$\begin{bmatrix} U_d \\ U_q \\ U_0 \end{bmatrix} = \frac{2}{3} T \begin{bmatrix} U_a \\ U_b \\ U_c \end{bmatrix} \tag{2.11}$$

Where T is:

$$T = \begin{bmatrix} \cos\theta & \cos\left(\theta - \frac{2\pi}{3}\right) & \cos\left(\theta + \frac{2\pi}{3}\right) \\ \sin\theta & \sin\left(\theta - \frac{2\pi}{3}\right) & \sin\left(\theta + \frac{2\pi}{3}\right) \\ 0.5 & 0.5 & 0.5 \end{bmatrix} \tag{2.12}$$

Thus, the 3-phase stator voltages in d-q reference frame are given by [46]:

$$\begin{bmatrix} V_d \\ V_q \\ V_0 \end{bmatrix} = \frac{2}{3} \begin{bmatrix} \cos\theta & \cos\left(\theta - \frac{2\pi}{3}\right) & \cos\left(\theta + \frac{2\pi}{3}\right) \\ \sin\theta & \sin\left(\theta - \frac{2\pi}{3}\right) & \sin\left(\theta + \frac{2\pi}{3}\right) \\ 0.5 & 0.5 & 0.5 \end{bmatrix} \begin{bmatrix} V_a \\ V_b \\ V_c \end{bmatrix} \tag{2.13}$$

Here, λ_q and λ_d are q-axis and d-axis flux-linkages respectively, which can be written in the following way:

$$V_{sd} = R_s I_d + \frac{d(L_d I_d + \lambda_{pm})}{dt} - \omega_e L_q I_q \tag{2.14}$$

$$V_{sq} = R_s I_q + \frac{d(L_q I_q)}{dt} + \omega_e(\lambda_{pm} + L_d I_d) \tag{2.15}$$

Here, L_q and L_d are q-axis and d-axis inductances.

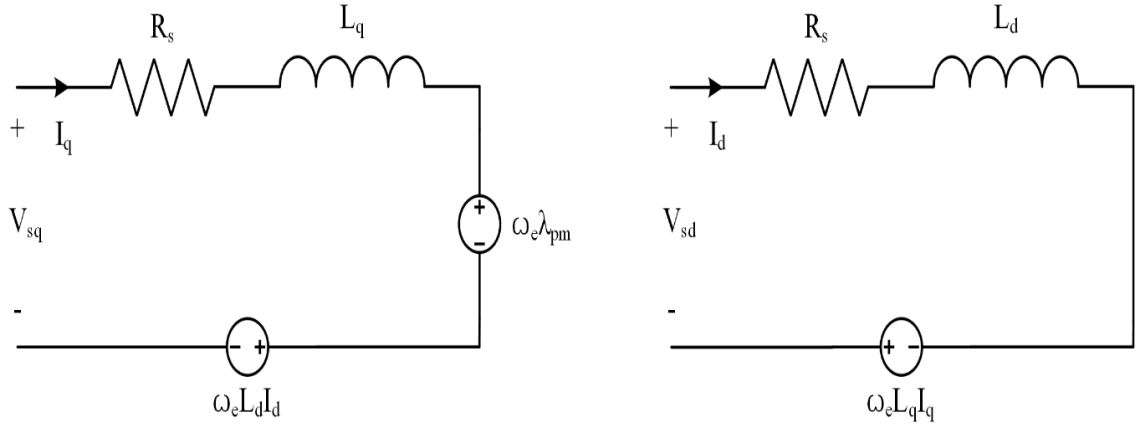

Fig.2.2: Equivalent circuit of PMSM in d-q frame.

Fig. 2 shows the dynamic equivalent circuit of PMSM in d-q frame. In the steady state at a constant speed λd and λq become time independent, hence, $\frac{d\lambda_d}{dt}$ and $\frac{d\lambda_q}{dt}$ can be eliminated from the formulation. If the stator resistance is negligible or neglected, it follows that the PMSM model can be represented by a standard mathematical model in the d-q frame as follows [47]:

At steady-state, the time dependent components become zero and if the stator resistance is negligible then the voltage equations of PMSM in d-q frame at steady-state is given by:

$$V_{sd} = -\omega_e L_q I_q \tag{2.16}$$

$$V_{sq} = \omega_e(\lambda_{pm} + L_d I_d) \tag{2.17}$$

Assuming the motor losses negligible, the output power of PMSM in d-q frame is given by:

$$P_{out} = \frac{3}{2}(V_{sd} I_d + V_{sq} I_q) \tag{2.18}$$

Substituting the equations (2.16) and (2.17) into (2.18), yields:

$$P_{out} = \frac{3}{2}\omega_e(\lambda_{pm} I_q + (L_d - L_q) I_d I_q) \tag{2.19}$$

Also, the electrical speed of motor is given by:

$$\omega_e = \frac{P}{2}\omega_m \tag{2.20}$$

Where, $\frac{P}{2}$ is number of pole-pairs.

From the output power and motor speed expression presented in equations (2.19) and (2.20), the developed torque relation is given by:

$$T_d = \frac{P_{out}}{\omega_m}\frac{3}{2}\frac{P}{2}(\lambda_{pm} I_q + (L_d - L_q) I_d I_q) \tag{2.21}$$

It is evident from the torque expression of PMSM that it is a combination of "reluctance torque" (due to difference in q-axis and d-axis inductance values) and "magnet excitation torque" (due to permanent magnets).

However, the torque expression for SPMSM has magnetic excitation torque only because of its no saliency $(L_d = L_q)$.

The dynamic mechanical equation of PMSM can be written in the following way:

$$T_d = T_l + J\frac{d\omega_m}{dt} + B\omega_m \tag{2.22}$$

Here, J is rotor's moment of inertia, B is viscous friction coefficient and T_l is load torque.

2.3 CONTROL METHODS FOR PMSM

The primary objective of any motor control technique is to achieve the required reference speed and for that purpose the output torque delivered by the motor needs to be controlled. The three widely used control methods for PMSM drives are:

- V/f control
- Direct torque control (DTC)
- Field-oriented control (FOC)

The V/f control method is cost-effective and easier to implement. Generally, the V/f method is implemented for the open-loop controls only. Hence, the encoder or resolver isn't needed here. Because of the inability to control torque, the V/f method isn't feasible for high performance drives.

Out of these three-control techniques, FOC will be the most effective option for applications which requires fast dynamic response and high-performance. Typically, FOC is a dual closed loop control technique and in which an encoder or resolver is required for speed sensing in outer speed control loop. While, inner control loop is the current control loop and it indirectly controls the torque. Therefore, FOC has precise speed control and faster dynamic response. However, if sensorless approach is adopted then encoder or resolver won't be required which in turn reduces the implementation cost for this control method.

DTC aims to merge the torque and flux control into a single switching algorithm rather than controlling the torque through current controller as in FOC [25]. Out of these control techniques, DTC provides the fastest torque response. In DTC, field orientation does not require the speed feedback. The main disadvantage of DTC is variable switching frequency with high torque ripples due to use of hysteresis controller.

The main aim of the FOC algorithm is to regulate the phase and amplitude of stator current phasor, $\vec{I}_s$, in order to achieve the desired torque and speed response. Fig. 2.4 shows the FOC control scheme for the PMSM drive system. The control scheme consists two control loops, namely, the outer speed loop ensures that the reference speed command is followed by the drive while the inner current control loop ensures that desired torque demand is achieved which is the output of speed controller. Usually, the speed

controller design relies on the nature of control algorithm whereas the current controller design is based on the machine parameters.

There are numerous control techniques used for conventional FOC method, including the MTPA and flux-weakening strategies [18–20]. In traction application, MTPA control is optimum for low-speed operation whereas for high-speed operation flux-weakening control is needed. Though the flux-weakening and MTPA control employs various algorithms, they are fundamentally FOC approaches.

2.3.1 MTPA Control Algorithm

To generate maximum torque at a given current value, the torque angle "β" has to be controlled. In order to find the torque angle corresponding to maximum torque "β_{max}", the torque expression for permanent magnet motors has to be analysed.

As Surface mounted permanent magnet (SPM) motors have no saliency, d-axis and q-axis phase inductances are equal, therefore reluctance torque is absent. The torque expression for SPM motors can be written as:

$$T_d = \frac{3}{2}\frac{P}{2}\lambda_m I_q \tag{2.23}$$

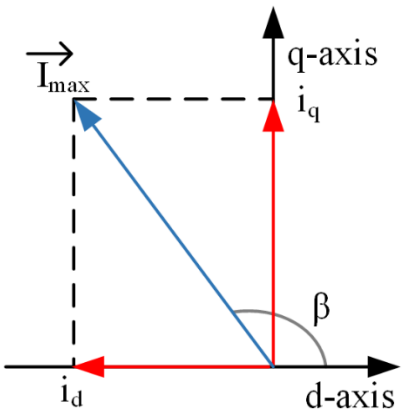

Fig.2.3: Torque Angle

From the Fig. 2.3, we can write:

$$I_d = I_s \cos\beta \tag{2.24}$$

$$I_q = I_s \sin\beta \tag{2.25}$$

where, I_s is the amplitude of the peak stator phase current and β is the torque angle which typically lies in the range 90° to 180°.

By substituting the equation (2.25) into the torque expression in (2.23), we can obtain the following:

$$T_d = \frac{3}{2}\frac{P}{2}\lambda_m I_s \sin\beta \tag{2.26}$$

The torque angle which outputs the maximum torque can be obtained by equating the derivative of the torque with respect to β in (2.26) to 0,

$$\frac{dT_d}{d\beta} = 0 \tag{2.27}$$

$$\frac{dT_d}{d\beta} = \frac{3}{2}\frac{P}{2}\lambda_m I_s \cos\beta = 0 \tag{2.28}$$

Using expression (2.24) in (2.28), we can obtain the following:

$$\frac{3}{2}\frac{P}{2}\lambda_m I_d = 0 \tag{2.29}$$

$$I_d = 0 \tag{2.30}$$

Since, $I_s^2 = I_d^2 + I_q^2$, then I_q can be written as follows:

$$I_q = \sqrt{I_s^2 - I_d^2} \tag{2.31}$$

Using (2.29) and (2.30), we can obtain the I_q for MTPA control as follows:

$$I_q = I_s \tag{2.32}$$

Thus keeping $I_{q\_MTPA} = I_s$ and $I_{d\_MTPA} = 0$ is the most suitable approach to generate maximum torque in SPM motor.

Now the torque angle, $\beta_{\max}$, for the maximum torque condition in SPMSM is given by,

$$\beta_{max} = \tan^{-1}\left(\frac{I_{q\_MTPA}}{I_{d\_MTPA}}\right) \tag{2.33}$$

$$\beta_{max} = 90° \tag{2.34}$$

However, in the vector control strategy used for this PMSM drive, the q-axis current reference is set by the outer speed loop based on the reference torque demand. Thus the I_{q_ref} can be written as follows:

$$I_{q\_ref} = \frac{T^{ref}}{\frac{3P}{22}\lambda_m} \tag{2.35}$$

Therefore, for the MTPA control of SPM motors, the modified d- and q-axis currents with saturation limits can be expressed from the above information as follows:

$$I_{d\_sat} = I_{d\_MTPA} \tag{2.36}$$

$$I_{q\_sat} = min\left(I_{q\_ref},\ I_{q\_MTPA}\right) \tag{2.37}$$

From (2.36) and (2.37) it is evident that, for every supply current value, there exists a particular combination of d-axis and q-axis currents that results in the maximum torque operation and maximum torque angle is dependent on supply current value.

Base Speed Calculation

Base speed is described as the maximum attainable speed at which rated current is drawn by the motor at a given supply voltage outside the field weakening region. In other words, at this point phase voltage needed to supply rated current is equal to the available supply voltage.

The inverter voltage constraints are given by:

$$V_{sd}^2 + V_{sq}^2 \leq V_{max}^2 \tag{2.38}$$

and,

$$V_{max} = \frac{V_{dc}}{\sqrt{3}} - R_s I_{max} \tag{2.39}$$

where, V_{max} is the maximum fundamental line to neutral voltage (peak) supplied to the motor (Volts) and I_{max} is the maximum phase current (peak) of the motor (Amperes).

Using the steady-state FOC equations in the d-q reference frame:

$$V_{sd} = I_d R_s - \omega_e L_q I_q \tag{2.40}$$

$$V_{sq} = I_q R_s + \omega_e L_d I_d + \omega_e \lambda_{pm} \tag{2.41}$$

Where, I_q is the d-axis phase current corresponding to MTPA (Amperes).

I_d is the d-axis phase current corresponding to MTPA (Amperes).

Using equations (2.38) using (2.40) and (2.41) and substituting corresponding MTPA d and q-axis phase current values, $I_{q\ (mtpa)} = I_{max}$ and $I_{d\ (mtpa)} = 0$, gives:

$$(-\omega_{BS} L_s I_{max})^2 + \left(I_{max} R_s + \omega_{BS} \lambda_{pm}\right)^2 = V_{max}^2 \tag{2.42}$$

Solving this quadratic equation for base speed ω_{BS} before field weakening is applied, gives solutions:

$$\omega_{BS\ (motoring)} = \frac{-2\lambda_{pm} I_{max} R_s + \sqrt{\left(2\lambda_{pm} I_{max} R_s\right)^2 - 4\left(\lambda_{pm}^2 + (L_s I_{max})^2\right)\left((I_{max} R_s)^2 - V_{max}^2\right)}}{2\left(\lambda_{pm}^2 + (L_s I_{max})^2\right)} \tag{2.43}$$

$$\omega_{BS\ (braking)} = \frac{-2\lambda_{pm} I_{max} R_s - \sqrt{\left(2\lambda_{pm} I_{max} R_s\right)^2 - 4\left(\lambda_{pm}^2 + (L_s I_{max})^2\right)\left((I_{max} R_s)^2 - V_{max}^2\right)}}{2\left(\lambda_{pm}^2 + \left(L_q I_{max}\right)^2\right)} \tag{2.44}$$

2.3.2 Field-Weakening Control Algorithms

As back-EMF is directionally proportional to the motor speed and air gap flux, hence with the increasing speed back-EMF also increases. At one-point maximum output voltage of the drive and back-EMF becomes equal, thereby unable to draw more armature current and hence no further torque can be produced. Therefore, for wide speed range, air-gap flux has to be reduced.

In field-weakening operation, a negative d-axis current is injected in the stator to establish a demagnetizing MMF which will negate the MMF due to PMs placed on the rotor. This results in the weakening of resultant air-gap flux and hence a wide speed range can be attained by implementing flux-weakening control.

There are several flux-weakening control algorithms used for SPMSM. However, the most widely used flux-weakening algorithms for SPMSM are:

1. Constant voltage constant power control
2. Voltage and current limited flux-weakening control

1. Constant-voltage-constant-power (CVCP) control:

As the title itself indicates, this approach maintains the voltage and power constant by forcing current phasor to follow constant power trajectory. However, in the vector control strategy used for this PMSM drive, the q-axis reference current is set by

the outer speed loop based on the reference torque demand. Thus, only the *d*-axis reference current is calculated by the CVCP algorithm.

Then I_{q_fw} and I_{d_fw} can be written as follows:

$$I_{q\_fw} = \frac{T^{ref}}{\frac{3P}{22}\lambda_m} \tag{2.45}$$

As a constant voltage operation, q-axis voltage needs to be constant while as a constant power operation, the q-axis voltage component value should be kept at the base speed., which can be expressed as follows:

$$V_q = V_{qb} = constant \tag{2.46}$$

The component at the base speed is expressed by the MTPA operation conditions, $I_d = 0$ for SPM motors, as base speed is described as the maximum attainable speed outside the field weakening region.

$$V_{qb} = \omega_{BS}\lambda_m \tag{2.47}$$

Substituting, $V_q = \omega_e(\lambda_m + L_d I_d)$ and (2.47) into (2.46), we can get the following:

$$\omega_e(\lambda_m + L_d I_d) = \omega_{BS}\lambda_m = constant \tag{2.48}$$

$$I_{d\_fw} = \frac{(\omega_{BS} - \omega_e)\lambda_m}{\omega_e L_d} \tag{2.49}$$

From the above information the d- and q-axis currents with saturation limits can be expressed as follows:

$$I_{d\_sat} = max\left(I_{d\_fw}, -I_{max}\right) \tag{2.50}$$

$$I_{q\_lim} = \sqrt{I_{max}^2 - I_{d\_sat}^2} \tag{2.51}$$

$$I_{q\_sat} = sat\left(I_{q\_fw},\ I_{lim}\right) \tag{2.52}$$

The saturation function used for determining I_{q_sat} is expressed as follows:

If $I_{q\_fw} < -I_{q\_lim}$, then $I_{q\_sat} = -I_{q\_lim}$

If $I_{q\_fw} > I_{q\_lim}$, then $I_{q\_sat} = I_{q\_lim}$

If $-I_{q\_lim} \leq I_{q\_fw} \geq I_{q\_lim}$, then $I_{q\_sat} = I_{q\_fw}$

2. Voltage and current constraint flux-weakening control:

Generally, all the flux-weakening control algorithms considers two constraints specifically the maximum current and maximum voltage. In a motor-drive system, the motor's thermal dissipation decides the current limitation while the limited DC bus voltage of the drive side decides the voltage limitation.

$$V_{sd}^2 + V_{sq}^2 \leq V_{s\_max}^2 \tag{2.53}$$

$$I_d^2 + I_q^2 \leq I_{s\_max}^2 \tag{2.54}$$

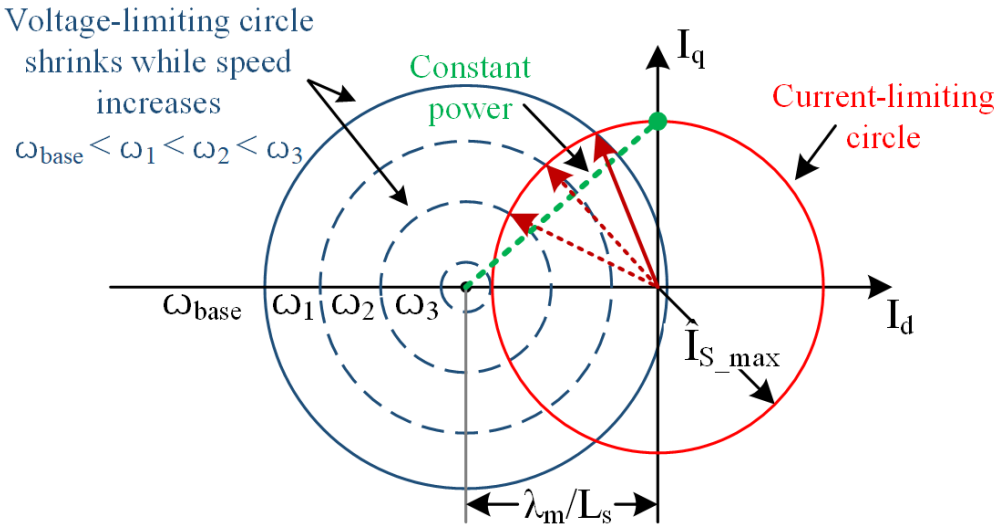

Fig.2.4: Voltage and Current limiting curves of SPMSM.

In above base speed operation, the reference currents generated for MTPA operation could not keep the maximum phase voltage within the voltage limitation. Hence, torque generation in flux-weakening control is limited by both voltage and current constraints.

Therefore, the reference currents for flux-weakening control are obtained by fulfilling both the critical conditions aforementioned in equation (2.53) and (2.54) and in order to maximize the torque, the phase voltage and supply current values will be kept at maximum level i.e., $\hat{V}_s = \hat{V}_{s\_max}$ and $\hat{I}_s = \hat{I}_{s\_max}$.

From current limitation given in equation (2.54), we can get,

$$I_q = \sqrt{\hat{I}_{s\_max}^2 - I_d^2} \tag{2.55}$$

Substituting the equation (2.16), (2.17) and (2.55) into the critical condition given in (2.53), yields the d-axis current for flux-weakening:

$$L_s^2\left(\hat{I}_{s\_max}^2 - I_d^2\right) + (L_s I_d + \lambda_m)^2 = \left(\frac{\hat{V}_{s\_max}}{\omega_e}\right)^2 \tag{2.56}$$

$$L_s^2 I_{s\_max}^2 - L_s^2 I_d^2 + L_s^2 I_d^2 + \lambda_m^2 + 2\lambda_m L_s I_d = \left(\frac{\hat{V}_{s\_max}}{\omega_e}\right)^2 \tag{2.57}$$

$$I_{d\_fw} = -\left(\frac{L_s^2 I_{s\_max}^2 + \lambda_m^2 - \left(\frac{\hat{V}_{s\_max}}{\omega_e}\right)^2}{2\lambda_m L_s}\right) \tag{2.58}$$

The q-axis current for flux-weakening is obtained by substituting the equation (2.58) back into (2.55),

$$I_{q\_fw} = \sqrt{\hat{I}_{s\_max}^2 - I_{d\_fw}^2} \tag{2.59}$$

From the above information the d- and q-axis currents with saturation limits can be expressed as follows:

$$I_{d\_sat} = max\left(I_{d\_fw}, -I_{max}\right) \tag{2.60}$$

$$I_{q\_lim} = \sqrt{I_{max}^2 - I_{d\_sat}^2} \tag{2.61}$$

$$I_{q\_sat} = sat\left(I_{q\_fw},\ I_{lim}\right) \tag{2.62}$$

The saturation function used for determining I_{q_sat} is expressed as follows:

If $I_{q\_fw} < -I_{q\_lim}$, then $I_{q\_sat} = -I_{q\_lim}$

If $I_{q\_fw} > I_{q\_lim}$, then $I_{q\_sat} = I_{q\_lim}$

If $-I_{q\_lim} \leq I_{q\_fw} \geq I_{q\_lim}$, then $I_{q\_sat} = I_{q\_fw}$

2.4 CONTROL SCHEME FOR SPMSM BASED ON CONVENTIONAL INVERTER

Fig. 2.5 shows the system configuration for implementing the field-oriented control strategy for MTPA and flux weakening operation of PMSM drive.

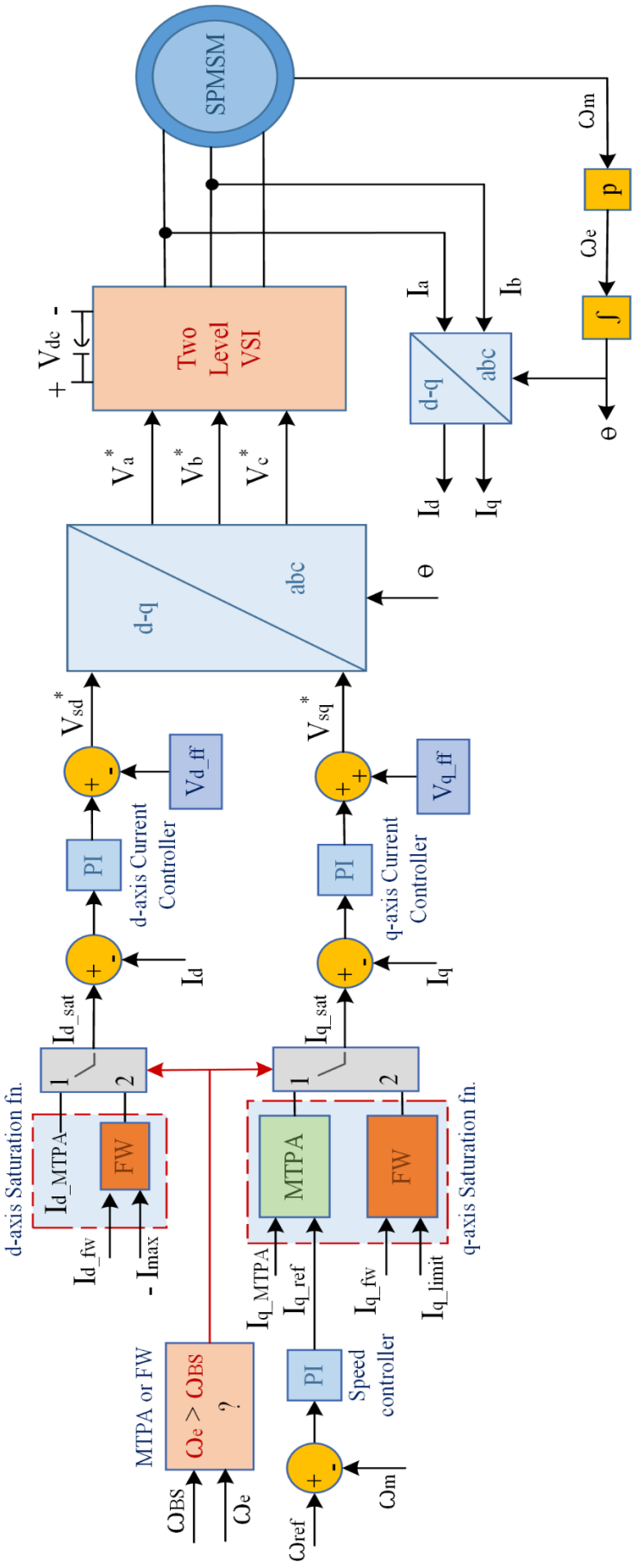

Fig.2.5: Vector control scheme for SPMSM based on conventional inverter.

As shown in Fig. 2.5, the operating mode of the drive is chosen based on the operational speed requirement. If below base speed operation is required MTPA control is opted otherwise flux-weakening operation is selected. The base speed is obtained from the steady state stator voltage equations while the motor speed is sensed. Using the MTPA and flux-weakening control algorithms, d-axis (I_{d_MTPA}, I_{d_fw}) and q-axis currents (I_{q_MTPA}, I_{q_fw}) are generated. The error signal generated from the outer speed loop serves as input to speed controller which outputs I_{qref}. Then the q-axis and d-axis currents generated from their respective control algorithms are limited by their saturation function, discussed in the controlling strategy. The operating region, MTPA or flux-weakening, is decided based on the decision whether the motor is required to operate above or below the base speed. Three phase stator winding currents are transformed into the d-q frame based on rotor angle (θ) acquired by integrating the electrical speed (ω_e) of the motor. Then based on the decision, the saturated q and d-axis currents (I_{q_sat}, I_{d_sat}) are then selected and compared with I_q and I_d. This error signal serves as input for inner current PI controllers, their outputs are then subjected to the feed-forward compensation to nullify the cross-coupling terms appear in d-axis and q-axis voltages and generates reference voltages [48]- [49], $V_{sd}^*$and V_{sq}^*. The q-axis feed-forward compensation component, V_{q_ff}, added in q-axis current controller output is given by ($L_s\omega_e I_d + \lambda_m\omega_e$) and d-axis feed-forward compensation component, V_{d_ff}, subtracted from d-axis current controller output is given by ($L_s\omega_e I_q$). The reference voltages thus obtained are transformed from d-q to abc reference frame which then serves as modulation signal to a conventional two-level inverter to produce suitable control pulses.

2.5 Simulation Results

A wide speed range vector controlled PMSM drive was simulated for three dynamic cases, specifically, load perturbation at constant speed, speed perturbation at given load and speed reversing at constant load. In constant torque zone, MTPA algorithm is implemented while in constant power zone, Voltage and current limited flux-weakening algorithm is implemented.

PMSM drive is supplied from a DC bus of 300 V and rating of parameters used in modelling of PMSM are listed in Table II. Maximum attainable phase voltage is set to 94 % of its absolute value to account for IGBT on state resistance and variations in

motor parameters due to temperature and saturation effects. Based on the given supply voltage and motor parameters, drive's base speed is calculated as 2120 rpm.

TABLE 2.1.

PMSM RATING

Rated Speed	3000 rpm
Rated Power	3.4 kW
Rated Current	6.9 A
Rated Torque	11 N-m
Poles	6
R_s	0.965 Ω
L_s	5.7 mH
J	0.0011 Kg-m^2
K_T	1.6 N-m/A rms
λ_m	0.2514 V-s
K_e	96.73 Vrms (L-L)/krpm

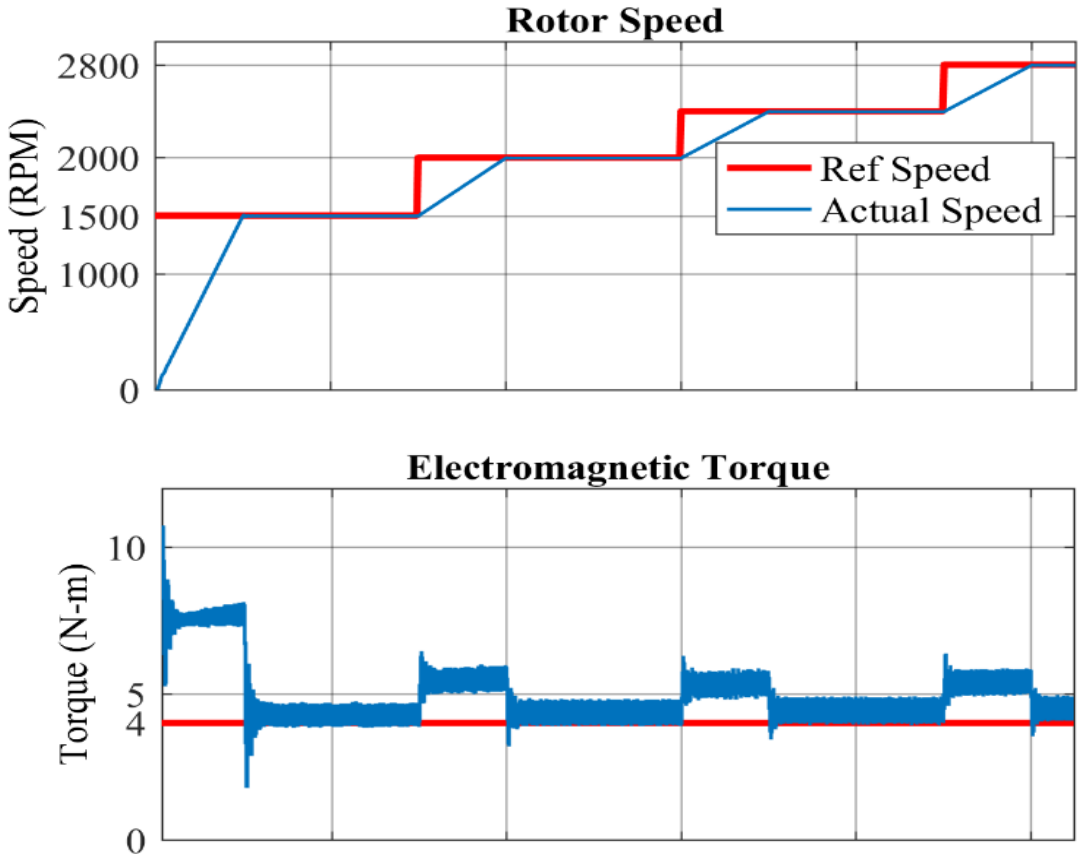

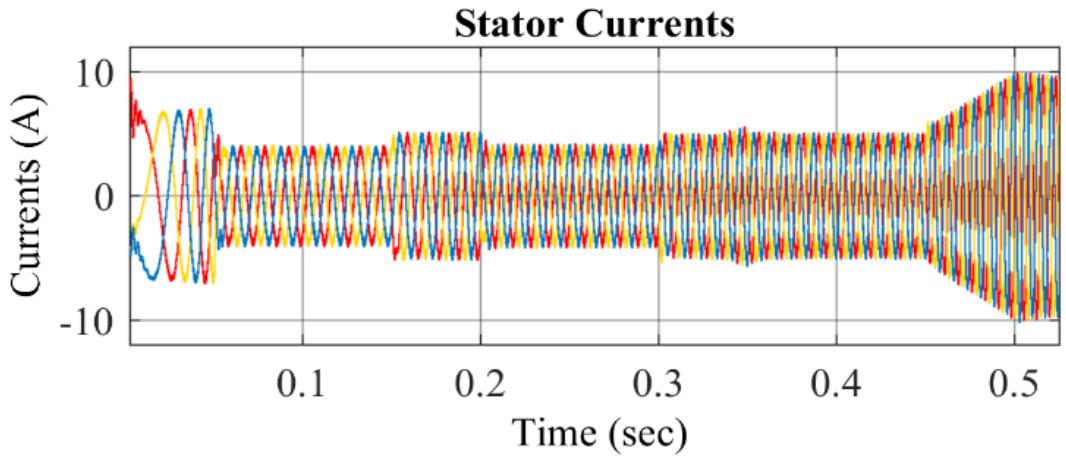

Fig.2.6: Speed perturbations at constant load.

Fig. 2.6 shows the dynamic performance of PMSM drive during speed perturbation. Initially, PMSM drive is started with 1500 rpm as reference speed at 4 N-m load. Then reference speed is perturbed, till the generated torque can meet the load demand, at interval of 0.15 sec. The drive successfully tracked the reference speed up to 2800 rpm, thus the speed range is extended by 32% at a load of 4 N-m. It delivers a constant load except during speed perturbations where torque level is increased in order to accelerate. Until the base speed, magnitude of the stator currents remains constant except for brief occasions during speed perturbation and then increases in flux-weakening region owing to increase in d-axis current. However, the frequency changes in accordance to the speed.

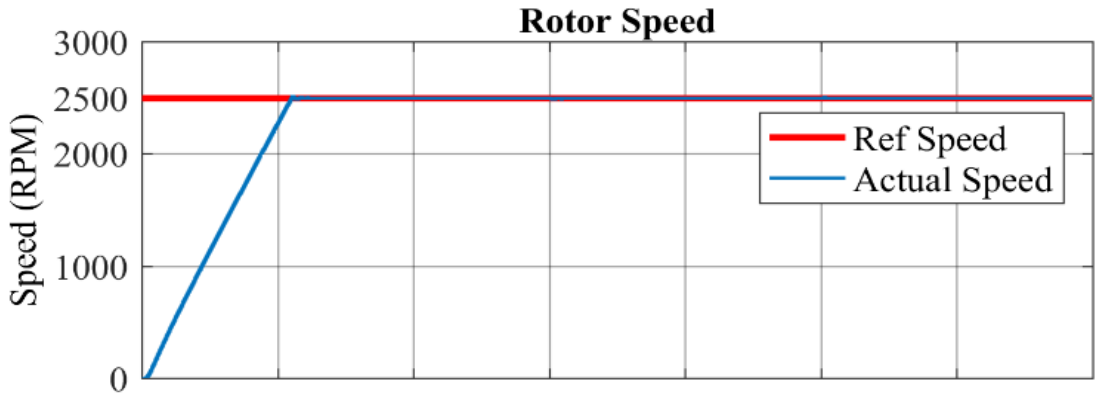

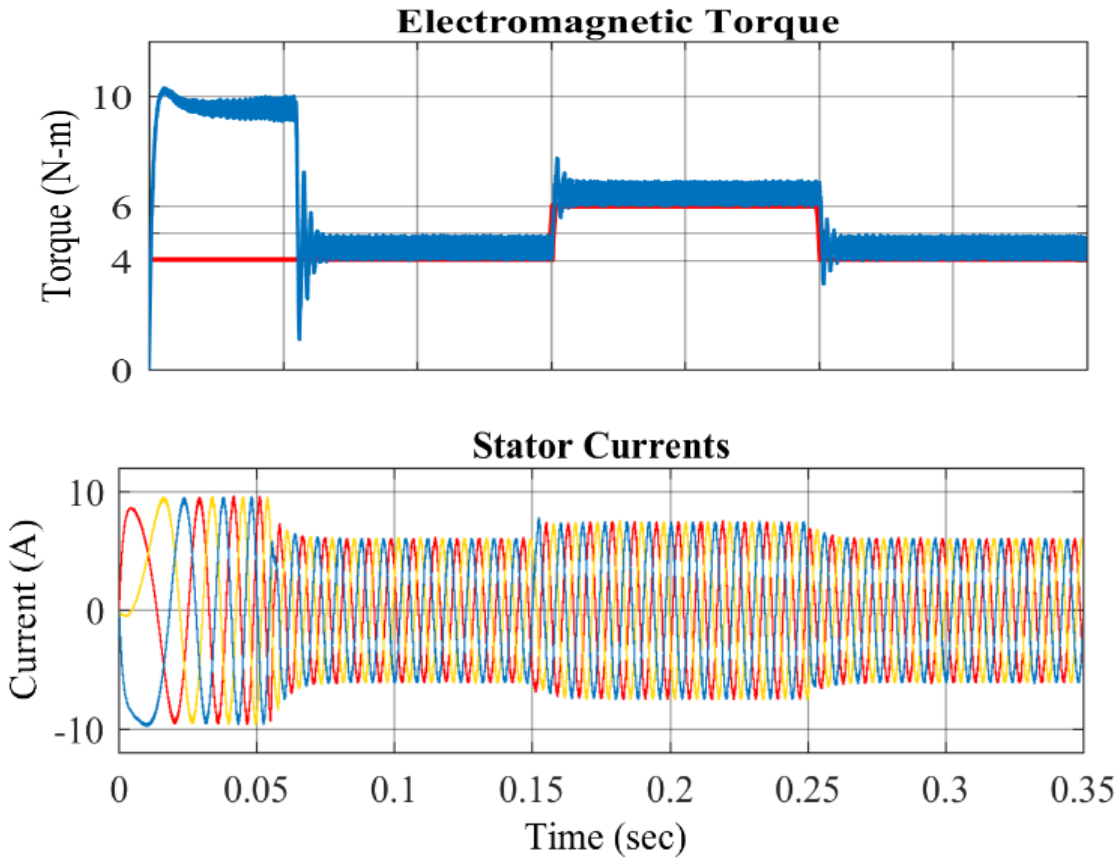

Fig.2.7: Load perturbations at constant speed.

Fig. 2.7 shows the dynamic performance of PMSM drive during load perturbation. Initially, PMSM drive is subjected to load of 4 N-m at a constant speed of 2500 rpm. Further, load torque is incremented by 2 N-m at 0.15 sec and then decreased by 2 N-m at 0.25 sec. PMSM drive successfully delivered the demanded torque and maintained the constant speed of 2500 rpm. The magnitude of stator currents changes in accordance with the load torque whereas the frequency remains constant due to constant speed operation.

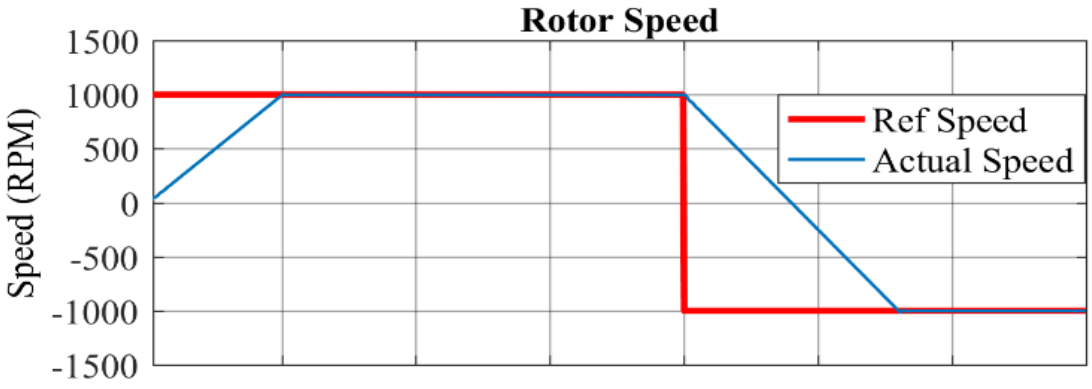

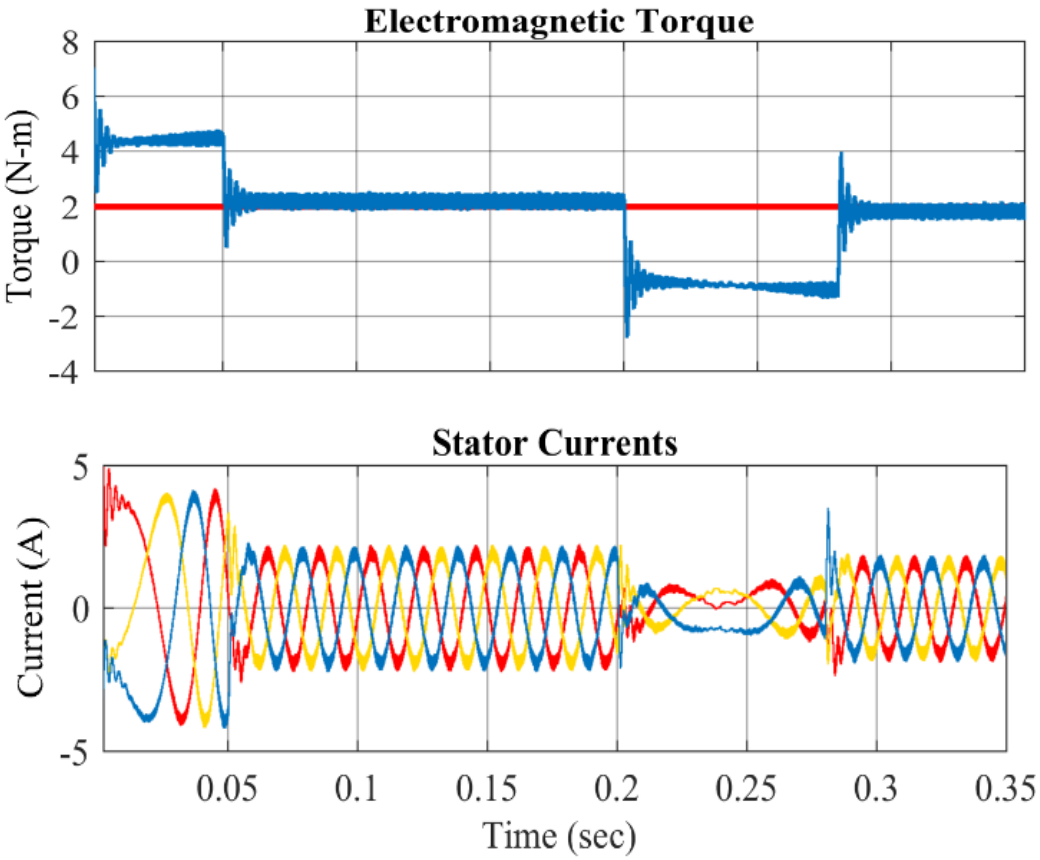

Fig.2.8: Speed reversal at constant load.

Fig. 2.8 shows the dynamic performance of PMSM drive during speed reversing. Initially, PMSM drive is started with 1000 rpm as reference speed at 2 N-m load then at 0.2 sec reference speed is reversed. The PMSM drive went through speed reversal from 1000 rpm to –1000 rpm effectively. It delivered a constant load except during brief intervals of initial acceleration and speed reversal, where torque changes in accordance with the direction of rotation. The magnitude and frequency of the stator currents remains constant except during intervals of initial acceleration and speed reversal. At the time of speed reversal, phase sequence of the current's reverses.

2.6 CONCLUSION

In this chapter, first in section 2.2 mathematical modelling of PMSM is demonstrated then in section 2.3 control methods of PMSM are introduced including MTPA and various flux-weakening techniques. In section 2.4 a wide speed range SPMSM drive control scheme aimed for providing the maximum efficiency and extended speed range operations is discussed and realized in MATLAB/Simulink environment. The

simulation result shows that, in MTPA control the PMSM drive is operating in optimum current way and demonstrates smooth transition between MTPA and flux-weakening control. The field weakening control shows stable response to the load torque disturbances and successfully achieves an extended speed range.

CHAPTER 3

Z-SOURCE INVERTER

3.1 INTRODUCTION

ZSI has a unique impedance circuit comprises of capacitors and inductors which couple dc link with the inverter's main circuit, as shown in fig. 3.1 This impedance networks allows ZSI to function as a buck-boost inverter [31].

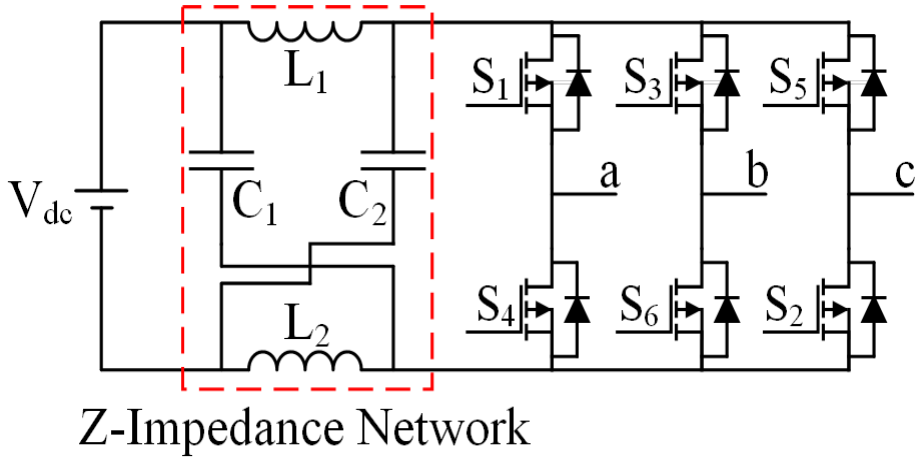

Fig.3.1: Z-Source Inverter.

A ZSI operates in two modes, namely the boost mode and normal mode. In normal mode it works similar to a conventional SPWM inverter whereas in boost mode, by using its shoot-through states it can directly boost the dc bus voltage. The shoot-through operation gives ZSI its voltage boosting capability by turning on both the switches of same leg simultaneously which results in the charging of inductors present in the impedance network.

ZSI has many advantages over a conventional inverter which includes the voltage boosting ability, improved harmonic spectrum, improved power factor and ride-through capability during voltage sags [31]. Additionally, it eliminates the risk of shoot-through which will do a fatal harm in conventional voltage source inverter [31].

Voltage boost capability can also be achieved by implementing a two-stage conventional inverter, where dc bus voltage is boosted using a dc-dc converter. Although in comparison to ZSI based drives, such drives require additional switching device for

dc-dc converter, big size capacitors owing to increase in dc bus voltage and offers lower efficiency. Hence, ZSI based drives are better option.

TABLE-3.1.

PERMISSIBLE SWITCHING STATES OF ZSI

Switch	**Active states**						**Zero states**		**Shoot-through states**						
S_I	1	1	0	0	0	1	0	1	1	0	0	1	1	0	1
S_4	0	0	1	1	1	0	1	0	1	0	0	1	1	0	1
S_3	0	1	1	1	0	0	0	1	0	1	0	1	0	1	1
S_6	1	0	0	0	1	1	1	0	0	1	0	1	0	1	1
S_5	0	0	0	1	1	1	0	1	0	0	1	0	1	1	1
S_2	1	1	1	0	0	0	1	0	0	0	1	0	1	1	1

The control techniques for ZSI are special because of its unique shoot-through states. Apart from the two zero and six active states, ZSI has seven possible shoot-through states shown in Table-2 which has to implement in the PWM

control. Out of these seven shoot-through states, shoot-through implemented using all three-phase leg generates least losses. The most widely used techniques for controlling ZSI are, namely, maximum boost method [42], maximum constant boost method [41] and simple boost method [35]. In this work ZSI is controlled using the maximum boost technique because of its merits over other techniques, including least voltage stress on switching device and highest voltage gain [50].

3.2 OPERATING PRINCIPLE OF ZSI

The ZSI has same operating principle to that of a dc-dc boost converter which boosts the output voltage by utilizing a charged inductor and then maintains the output voltage constant using a capacitor. Therefore, in order to obtain the voltage boosting abilities a charged inductor is essential. As a result, a unique mode of operation called shoot-through mode is implemented on the inverter, which simultaneously turns on both the switching devices of the same phase leg in inverter and shorts the load. In shoot-through state, because of the shorting of load the inductor begins charging. The shoot-

through operation isn't allowed in conventional inverter as this will results in the short-circuiting of dc bus.

As shoot through states are needed in ZSI, then total operating states in 3-phase ZSI increases to nine, that comprises one shoot-through state, two zero states and six active states. The nine permissible operating states of ZSI are presented in Table 3.1. From Table 3.1 it is clear that there are seven possible ways to generate shoot-through states, which are produced either by shorting the one phase leg or the combination of any two or all phase legs. However, the least conduction losses are offered during the shoot-through when all three phase legs are shorted.

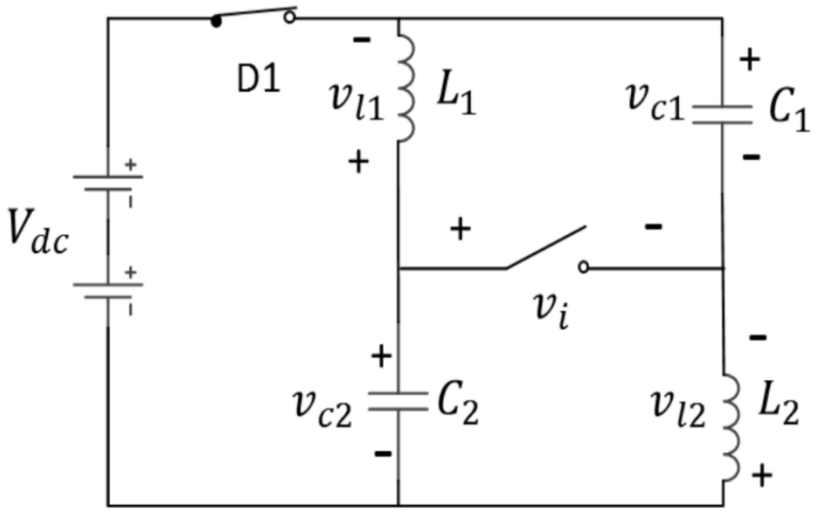

(a) Zero state

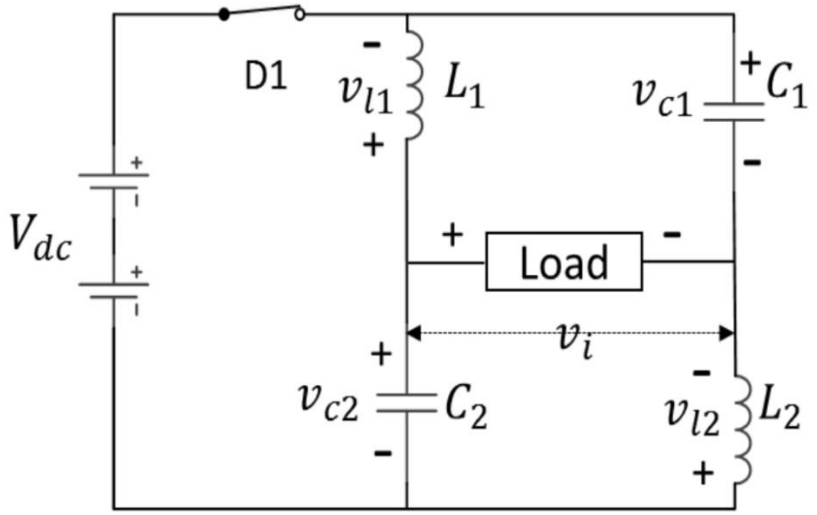

(b) Active state

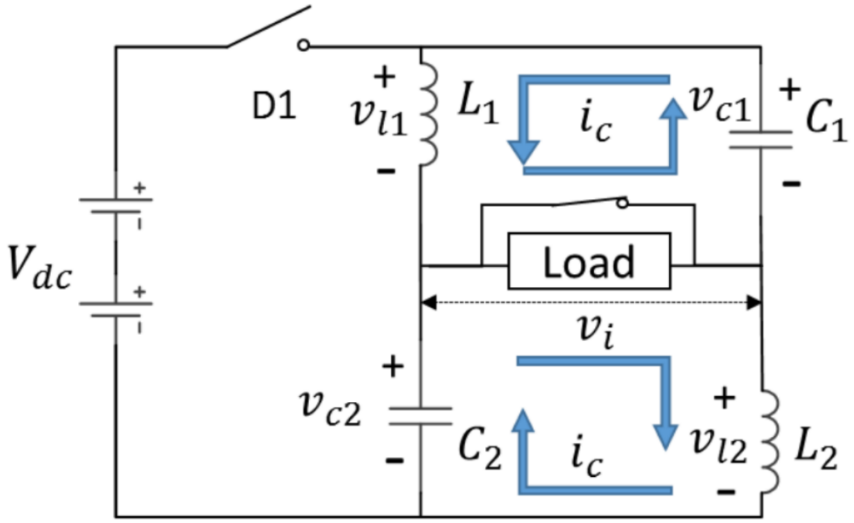

(c) Shoot-Through state

Fig.3.2: Equivalent circuit of ZSI.

Fig. 3.2 (a) shows the zero-state operation of ZSI, in this mode the load is open-circuited which means that inductors will discharge and at steady state the inductor currents will drop to zero. In addition, during zero-state capacitors are charging. Here, diode, D_1, conducts till the current through inductor decreases to zero and at that instant capacitor will be charged fully to its peak value.

Fig. 3.2 (b) shows the active-state operation of ZSI, in this mode both the inductors will discharge and diode, D_1, keep conducting. Therefore, during discharging the inductor currents will continue to drop and both the inductors become voltage sources in order to sustain the current flow. In active-state, the voltage across the inverter bridge is same as the output voltage of Z-source network.

Therefore, the voltage across the Z-source network, v_i, is given by:

$$v_i = V_{dc} + v_{l1} + v_{l2} \tag{3.1}$$

From equation (3.2), it is clear that in active-state output voltage exceeds the dc bus. Assuming the symmetrical Z-impedance network, i.e.,

$$v_{l1} = v_{l2} \quad and \; v_{c1} = v_{c2} \tag{3.2}$$

The voltage across the inductors and capacitors of ZSI during active-state will be:

$$v_{l1} = v_{l2} = v_{la} \qquad v_{c1} = v_{c2} = v_{ca} \tag{3.3}$$

From KVL, the relation between capacitor voltage, v_{ca}, and inductor voltage, v_{la}, is given by:

$$v_{la} = v_{ca} - V_{dc} \tag{3.4}$$

Using equations (3.3) and (3.4) in (3.1), we get:

$$v_i = V_{dc} + 2v_{la} = 2v_{ca} - V_{dc} \tag{3.5}$$

Fig. 3.2 (c) shows the shoot-through state operation of ZSI, in this mode the load is short-circuited and diode, D_1, stops conducting. Also, the capacitor C_1 and C_2 which are fully charged during the zero-state will starts discharging through the inductors L_1 and L_2 respectively. Therefore, the inductors are charging in shoot-through mode which are required for the voltage boosting operation of ZSI. Moreover, it is clear that only half of the charging current will flow through the phase legs if both the phase-legs are shorted which verifies that shoot-through state produced by shorting all phase legs results in the least conduction loss across the switching devices.

The voltage across the Z-source network, v_i, is given by:

$$v_i = 0 \tag{3.6}$$

The voltage across the inductors and capacitors of ZSI during shoot-through state will be:

$$v_{l1} = v_{l2} = v_{ls} \qquad v_{c1} = v_{c2} = v_{cs} \tag{3.7}$$

and,

$$v_{l1} = v_{c1} \qquad v_{l2} = v_{c2} \tag{3.8}$$

Considering Capacitors in Z-impedance network are sufficiently large for maintaining the output voltage constant over the switching period, then the voltage across the capacitors in active and shoot-through states can be written as:

$$v_{ca} = v_{cs} = V_c \tag{3.9}$$

In steady-state, the average inductor voltage during a switching cycle must be zero. Therefore, the average voltage across the inductors can be written as follows:

$$\langle v_l \rangle = \frac{v_{ls}T_s + v_{la}T_a}{T} = 0 \tag{3.10}$$

Here, T_a and T_s, are time interval for active and shoot-through states respectively.

In steady-state operation, zero-state isn't considered. Thus, the switching time period, T, is given by:

$$T = T_a + T_s \tag{3.11}$$

Using equation (3.9) into (3.4), (3.7) and (3.8), we get:

$$v_{la} = V_c - V_{dc} \qquad v_{ls} = V_c \tag{3.12}$$

Substituting the equation (3.12) into (3.10), the average inductor voltage can be written as:

$$\langle v_l \rangle = \frac{V_{dc}T_s + (V_c - V_{dc})T_a}{T} = 0 \tag{3.13}$$

or,
$$\frac{V_c}{V_{dc}} = \frac{T_a}{T_a - T_s} \tag{3.14}$$

Similarly, the average voltage across the Z-impedance network is given by:

$$\langle v_i \rangle = \frac{\langle v_{is} \rangle T_s + \langle v_{ia} \rangle T_a}{T} = 0 \tag{3.15}$$

Here, $\langle v_{ia} \rangle$ and $\langle v_{is} \rangle$ is average voltage across the Z-impedance network during active and shoot-through states respectively.

From equations (3.5), (3.6) and (3.9), we can obtain:

$$\langle v_{is} \rangle = 0 \qquad \langle v_{ia} \rangle = 2V_c - V_{dc} \tag{3.16}$$

Substituting the equation (3.16) into (3.15), the average voltage across the Z-impedance network can be written as:

$$\langle v_i \rangle = \frac{(2V_c - V_{dc})T_a}{T} \tag{3.17}$$

Using the equations (3.11) and (3.14) into (3.17), we can obtain:

$$\langle v_i \rangle = \frac{\left(2V_c - \frac{T_a - T_s}{T_a} V_c\right) T_a}{T_a + T_s} = V_c = \frac{T_a}{T_a - T_s} V_{dc} \tag{3.18}$$

Using equations (3.14) and (3.16), the peak value of v_i is given by:

$$\hat{v}_i = v_{ia} = 2V_c - V_{dc} = \frac{T_a + T_s}{T_a - T_s} V_{dc} = K.V_{dc} \tag{3.19}$$

Here, K is the boost factor achieved by the implementing the shoot-through states.

From equation (3.11) boost factor, K, can be rewritten as:

$$K = \frac{T}{T_a - T_s} = \frac{1}{1 - 2\frac{T_s}{T}} \geq 1 \tag{3.20}$$

It is evident from the boost factor expression given in equation (3.20), if shoot-through time, T_s, is fixed to 0 then there will be no shoot-through states and the boost factor, B, becomes 1.

Hence, under this condition the ZSI will operate as conventional inverter without its voltage boosting ability. Additionally, the average voltage across the Z-impedance network, $\langle v_i \rangle$, will be same as the dc bus voltage, V_{dc}.

The peak output phase voltage of inverter, $\hat{v}_a$, in terms of peak voltage across the Z-impedance network, $\hat{v}_i$, is given by:

$$\hat{v}_a = M.\frac{\hat{v}_i}{2} \tag{3.21}$$

Here, M is the modulation index.

Since, peak voltage across the Z-impedance network, $\hat{v}_i$ is equivalent dc-bus voltage, V_{dc}. Therefore, on using equation (3.19) into (3.21), we can obtain:

$$\hat{v}_a = M.K\frac{V_{dc}}{2} = G.\frac{V_{dc}}{2} \tag{3.22}$$

Here, G is the voltage gain, whose value ranges from $0 < G < \infty$.

3.3 CONTROL METHODS FOR ZSI

The control methods used for ZSI are special compared to those used for conventional inverter because of its unique shoot-through states. Based on different pulse width modulation techniques, the most widely used methods for controlling the ZSI are,

- Simple boost method [31]
- Maximum boost method [42]
- Maximum constant boost method [41]

However, the maximum boost method has several merits over other methods, including the least voltage stress on switching device and highest voltage gain.

Maximum Boost Control

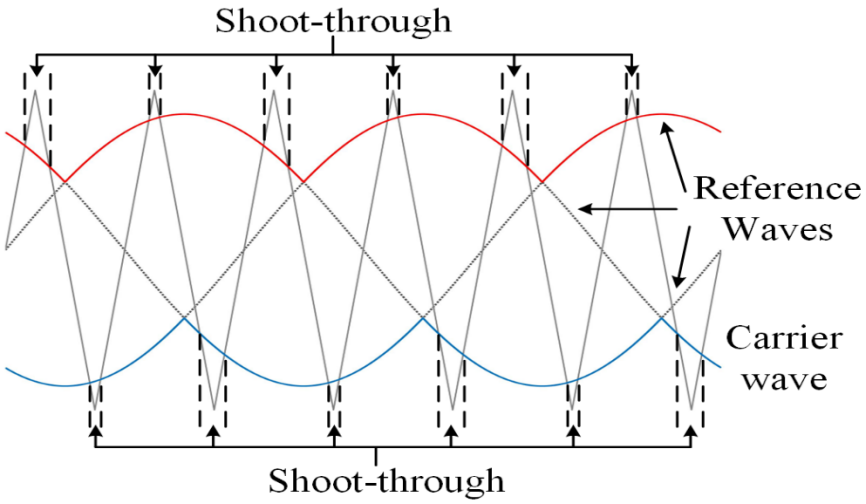

Fig.3.3: Maximum boost control of ZSI.

The maximum boost control shown in fig. 4, the instant when carrier signal value becomes either less than the minimum value of all three modulation signals or more than the maximum value of all three modulation signals, shoot-through control will be executed. Otherwise, the conventional PWM control is followed.

The above-mentioned control scheme is applicable till the modulation index, M, of modulation signals satisfies the criteria given in equation (3.23), else again conventional PWM control has to be followed.

$$\frac{\sqrt{3}\pi}{9} < M \leq 1 \tag{3.23}$$

The peak output phase voltage, $\hat{V}_o$, for maximum boost control, is given by [42]:

$$\hat{V}_o = M \cdot K \cdot \frac{V_{DC}}{2} = G \cdot \frac{V_{DC}}{2} \tag{3.24}$$

where, G is voltage gain and B is boost factor given by:

$$K = \frac{\pi}{3\sqrt{3}M - \pi} \tag{3.25}$$

The shoot-through duty ratio, d_s, for maximum boost control, which is the ratio of shoot-through time, t_s, by total time period, T_{sw}, ranges from 0 to 0.5 is given by:

$$d_s = \frac{2\pi - 3\sqrt{3}m_a}{2\pi} \tag{3.26}$$

The voltage stress, V_{stress}, on the switching devices for maximum boost control can be given as follows,

$$V_{stress} = K \cdot V_{DC} = \frac{\pi}{3\sqrt{3}m_a - \pi} V_{DC} \tag{3.27}$$

3.4 SIMULATION RESULTS

In order to validate the feasibility of control technique and analyse output voltage and current of ZSI, a ZSI model energising a balanced 3-phase RL load controlled using the maximum boost method is simulated in the MATLAB/Simulink environment. Additionally, the voltage stress across the switching devices and voltage gain provided by the aforementioned control method are also observed. The system parameters for the ZSI model are listed in Table-3.2.

Table-3.2

ZSI Parameters

DC Bus (V_{dc})		485 V
Z-Impedance Network	L_1	400 μH
	L_2	400 μH
	C_1	2200 μF
	C_2	2200 μF
R-L Load:	R	1 Ω
	L	3 mH
Switching Frequency (f_{sw})		5 KHz

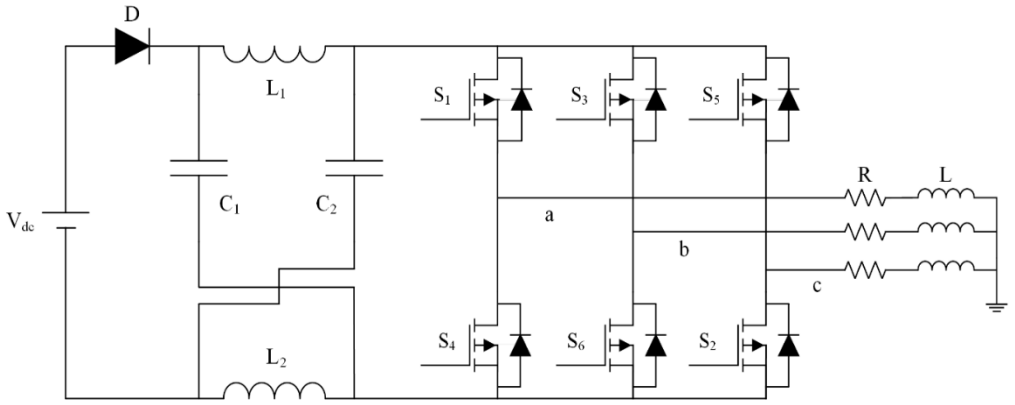

Fig.3.4: ZSI with balanced 3-phase RL load.

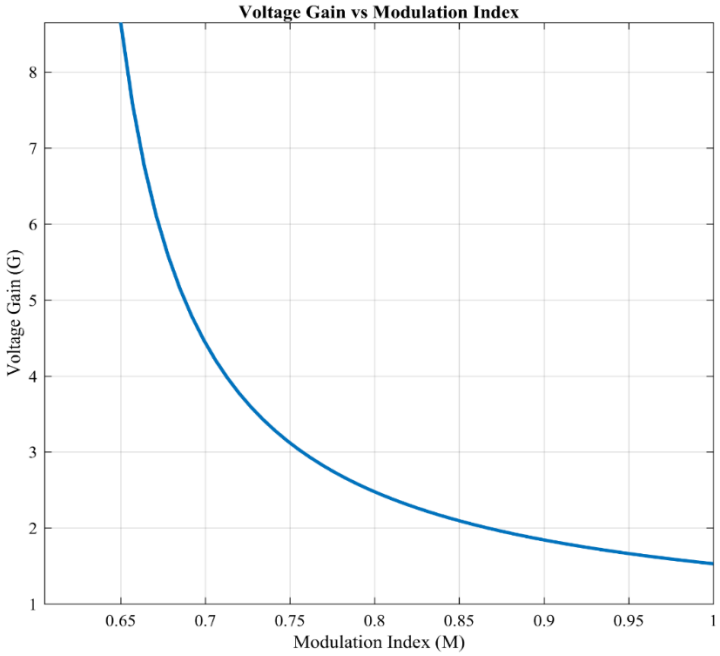

Fig.3.5: Voltage gain vs modulation index.

Fig. 3.5 shows the voltage gain, G, vs modulation index, M, for the maximum boost control. It is observed that the maximum achievable voltage gain of ZSI decreases with the increase in modulation index of reference signals which indicates the decrease in shoot-through time period, T_s.

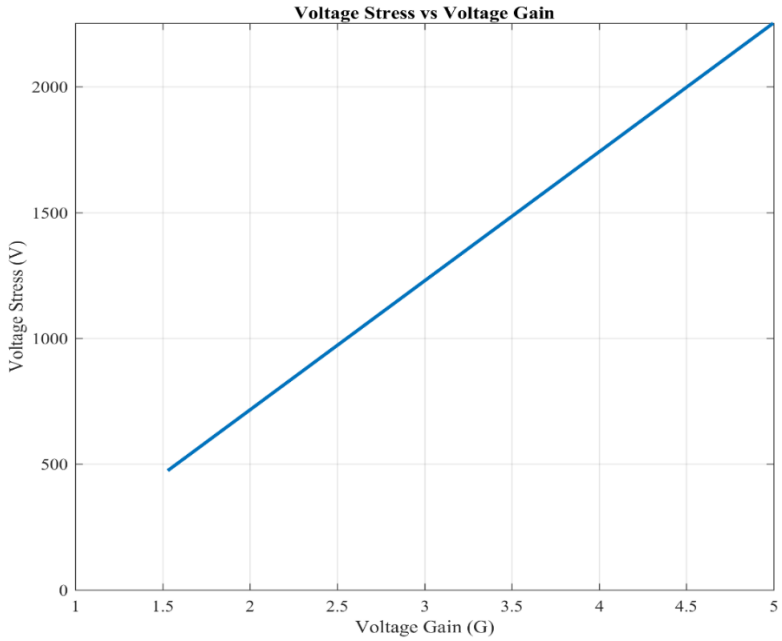

Fig.3.6: Voltage stress vs voltage gain.

Fig. 3.6 shows the voltage stress, V_{stress}, vs voltage gain, G, for the maximum boost control. It is observed that the voltage stress across the switching devices of inverter bridge rises with the increase in voltage gain provided by the ZSI. Therefore, it is obvious that higher voltage gain is achieved at the cost of large voltage stresses and for handling such large stresses high ratings switches will be required.

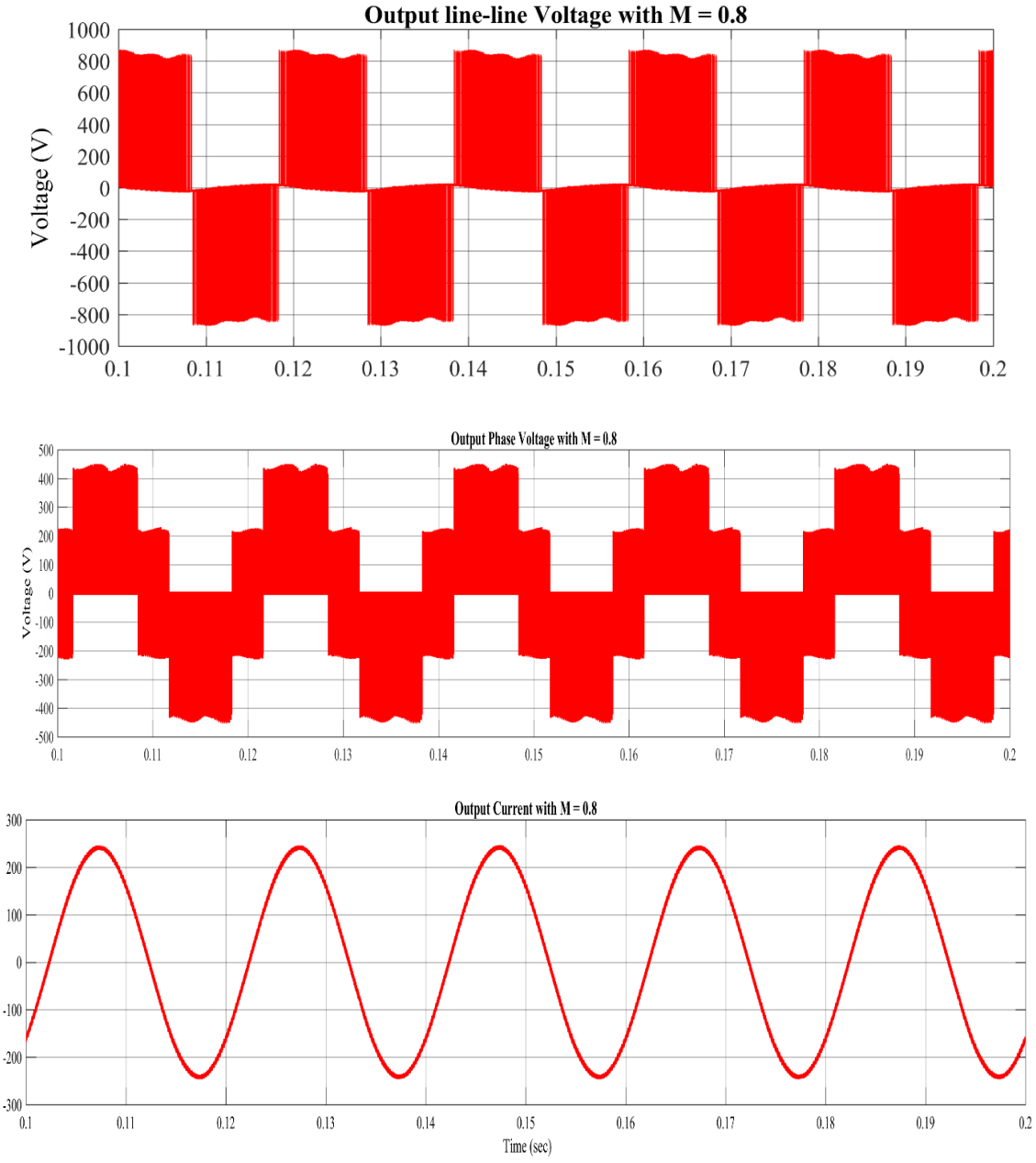

Fig.3.7: Output waveforms of ZSI for the maximum boost control.

Fig. 3.7 shows the output voltages and current waveforms of the ZSI for the maximum boost control with modulation index, $M = 0.8$. It is observed from the results

that line-line output voltage which has peak value of approximately 590 V exceeds the dc bus voltage level of 310 V. Hence, the voltage boosting capabilities of the ZSI are proved.

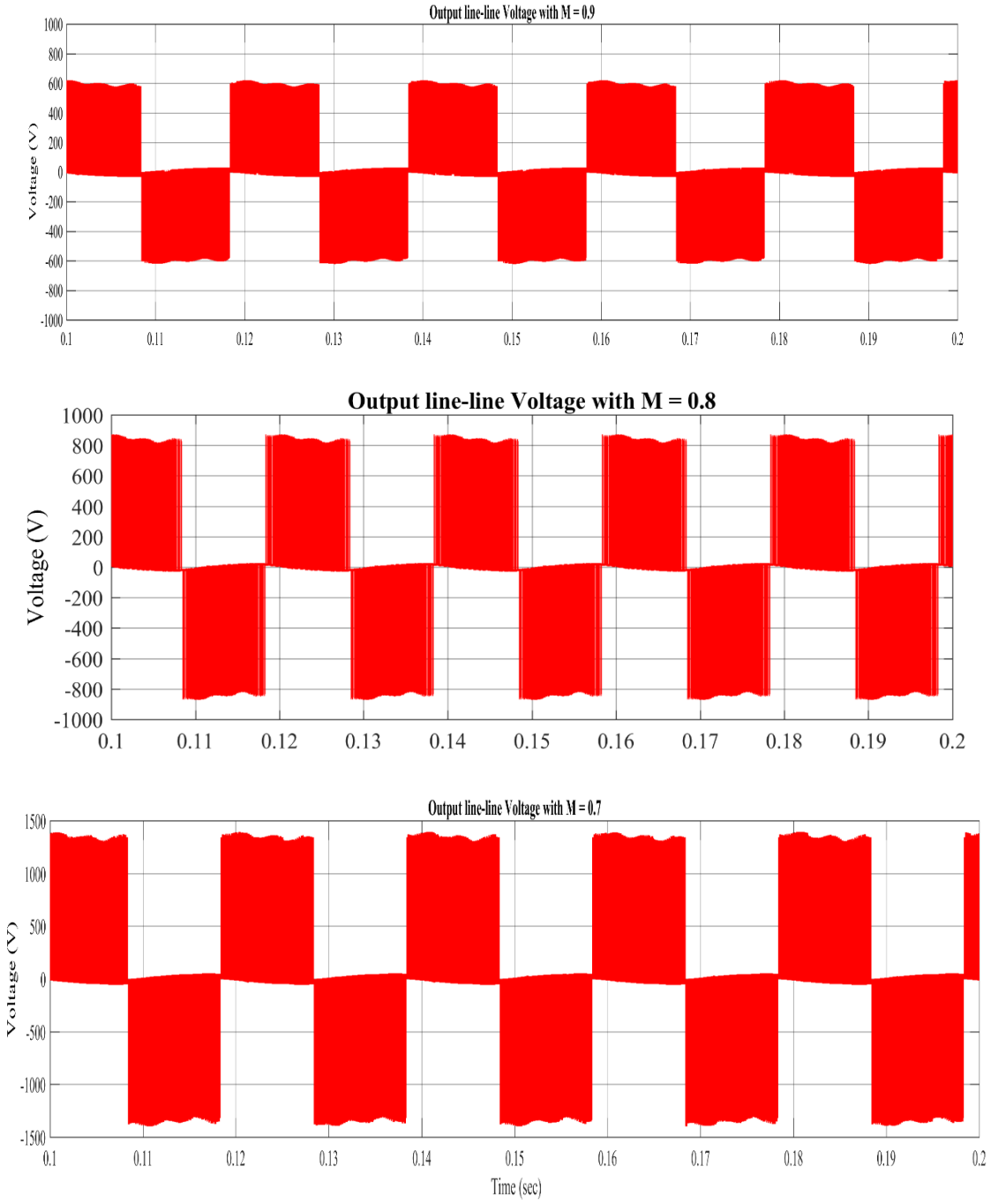

Fig.3.8: line-line output voltage waveforms of ZSI for different modulation indexes.

Fig. 3.8 shows the line-line output voltage waveform of ZSI with maximum boost control for different modulation indexes. From the decreasing peak values of line-line output voltage it is observed that the boost factor, which is the measure of how much times the voltage across Z-impedance network has increased, decreases with the increase in modulation index.

3.5 CONCLUSION

In this chapter, first in section 3.1 a brief introduction of the ZSI is presented then in section 3.2 the operating principle of the ZSI for different operating states, i.e., zero-state, active state and shoot-through state, is explained. Further, the analytical expression for the voltage gain and peak inverter output voltage has been obtained. In section 3.3 maximum boost control method for ZSI is explained and the maximum achievable voltage gain for the aforementioned control method is obtained. In section 3.4 in order to validate the feasibility of control technique and analyse the output waveforms, voltage gain and voltage stress across the switching devices a ZSI model with balanced 3-phase RL load using the maximum boost method is simulated in MATLAB/Simulink.

CHAPTER 4

BOOSTED VOLTAGE FLUX-WEAKENING CONTROL OF SPMSM based on ZSI

4.1 INTRODUCTION

The research on permanent magnet synchronous motor (PMSM) has drawn a lot of attention recently in various industrial applications, especially in electric vehicles (EV) due to its large torque-to-inertia ratio, smaller size, higher efficiency, high-power density and faster dynamic response [8].

Electrical drives in traction application requires wide CPSR operation, as shown in fig. 4.1. However, due to permanent magnets mounted on the rotor PMSM drives has small constant power speed range [2]. As back-EMF increases proportionally to the air gap flux and motor speed, therefore at one point back-EMF becomes equal to the drive's maximum output voltage. As a result, drive cannot draw more armature current, hence further torque generation is not possible and thereby motor speed cannot be increased without reducing the air-gap flux. Thus, to overcome this limitation, PMSM drives are operated with flux-weakening control for wide speed operation. In flux-weakening operation, the resultant air-gap flux is reduced by supplying negative d-axis stator current which will indirectly opposes the MMF (demagnetizing) produced by the permanent magnets mounted on the rotor.

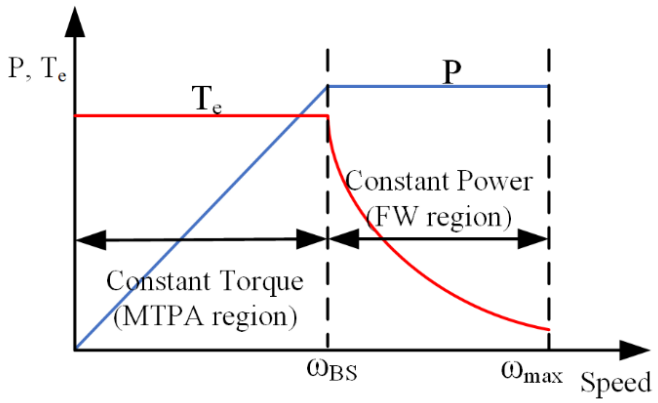

Fig.4.1: Typical torque/power vs speed curve of PMSM.

Some recent flux-weakening control methods for the control of PMSM drives has been discussed in the literatures. An outer stator voltage loop is implemented which

adjusts the current for flux-weakening control in order to prevent the saturation of current regulator in [23]. The performance of current controller is improved using a voltage command compensation in flux-weakening region in [24]. A current feedback control algorithm is implemented in flux-weakening operation using phase advance principle in [12]. Although all these controlling methods provides high-performance with fast dynamic response, they are limited by voltage constraint of the drive side. The maximum output voltage capability of a drive is crucial for deep flux-weakening operation.

To solve the above-mentioned issue of voltage constraint, a boosted voltage flux-weakening strategy is adopted in this work to expand the constant power speed range by utilizing the voltage boost ability of ZSI, that can output voltage significantly greater than the dc bus voltage [31]. In comparison to other conventional method, this boosted voltage flux-weakening control has no voltage constraint limitation and generates current reference which can maintain the output power constant. Additionally, a general flux-weakening algorithm based upon voltage and current constraints is studied and its performance is compared with the proposed flux-weakening scheme. The ZSI will operates in boost mode only during constant power region while in constant torque region it operates as conventional inverter [35]. In boost mode a special shoot through state control is employed and boost factor for ZSI is regulated by the voltage reference generated by the current controllers

4.2 BOOSTED VOLTAGE FLUX-WEAKENING ALGORITHM

The voltage limitation circle, shown in figure. 2.4, gradually shrinks with the increase in speed, which indicates that at deep flux-weakening operating region becomes smaller. However, if a drive has voltage boosting abilities, then the voltage limitation circle can be controlled.

The maximum attainable speed for a PMSM drive is given by:

$$\omega_{max} = \frac{\hat{V}_{s\_max}}{\sqrt{\left(L_s I_d + \lambda_{pm}\right)^2 + \left(L_s I_q\right)^2}} \tag{4.1}$$

It is apparent that, from equation (4.1), if a drive has voltage boosting abilities, then it is possible to further extend the maximum speed and, on this basis, a wide constant power speed range can be attained. Hence, instead of a conventional inverter, an inverter with voltage boosting ability is required like ZSI.

Generally, the boosted voltage control is applicable in both the flux-weakening zone and constant torque. Since maximum torque achieved in constant torque zone by implementing the MTPA operation has only current limitation. Therefore, the boosted voltage control has no effect in the constant torque zone. Though, the boosted output voltage from motor drive supports the generation of larger back-EMF and because of that the base speed will be further increased. Hence, with the boosted output voltage from drive it is possible to achieve the same speed range even without implementing the flux-weakening operation.

It is noticed from equation (4.1), increase in speed because of boosted voltage control in constant torque zone results in increase of maximum output voltage of motor drive by the same ratio. Whereas in flux-weakening zone, boosted voltage control has comparably slight increase in drive's maximum output voltage because of the negative d-axis current. Therefore, boosting the base speed to high levels by implementing the boosted voltage control in constant torque zone could cause large voltage stress on switching devices of motor drive. Additionally, at high-speed operation in application like EVs, requirement of torque isn't very high as compared to interval when vehicle starts. That's why implementation of boosted voltage control isn't suggested in the constant torque zone.

It is required to acquire an alternate flux-weakening strategy for the boosted voltage control because voltage and current constraints flux-weakening method is dependent on voltage limitation. The basic concept of BVFW control is to maintain the power output of PMSM drive constant and the operation is limited by the current constraint.

The output power expression for SPMSM is given by:

$$P_b = T_d \omega_m \tag{4.2}$$

Where, ω_m is mechanical speed of motor and P_b is rated output power available at the base speed. Using the torque relation from equation (2.33) in (4.2), the revised power expression is given by:

$$P_b = \left(\frac{3}{2}\frac{P}{2}\lambda_{pm} I_q\right) \omega_m \tag{4.3}$$

$$P_b = \frac{3}{2}\lambda_{pm} I_q \omega_e \tag{4.4}$$

Since, BVFW operation is limited by the current constraint. Using the current constraint given in equation (2.55) into (4.4), the speed dependent d-axis current for BVFW control is given by:

$$P_b = \frac{3}{2}\lambda_{pm}\left(\sqrt{\hat{I}_{s\_max}^2 - I_d^2}\right)\omega_e \tag{4.5}$$

$$I_d^2 = \left(\hat{I}_{s\_max}^2 - \frac{4}{9}\left(\frac{P_b}{\lambda_{pm}\omega_e}\right)^2\right)^2 \tag{4.6}$$

For flux-weakening operation, negative real root is chosen.

$$I_{d\_bvfw} = -\sqrt{\hat{I}_{s\_max}^2 - \frac{4}{9}\left(\frac{P_b}{\lambda_{pm}\omega_e}\right)^2} \tag{4.7}$$

Substituting the d-axis current given in equation (4.7) into (2.55), the q-axis current is given by:

$$I_{q\_lim} = \sqrt{\hat{I}_{s\_max}^2 - I_{d\_bvfw}^2} \tag{4.8}$$

From equation (4.8), it is obvious that I_{d_bvfw} will always be less than maximum peak phase current, $\hat{I}_{s\_max}$. That's why there is no need to limit it. However, q-axis need to be limited using the saturation function as follows:

I. If $I_{q\_ref} < -I_{q\_lim}$, then $I_{q\_bvfw} = -I_{q\_lim}$

II. If $I_{q\_ref} > I_{q\_lim}$, then $I_{q\_bvfw} = I_{q\_lim}$

III. If $-I_{q\_lim} \leq I_{q\_ref} \leq I_{q\_lim}$, then $I_{q\_bvfw} = I_{q\_ref}$

Since, BVFW control has no voltage limitation, it is recommended to operate the PMSM drive with this aforementioned control until the stator voltage becomes equal to the rated voltage for motor.

From equations (2.56) and (3.22), peak phase voltage at stator terminals and from the ZSI output are rewritten here as follows,

$$\hat{V}_s = \sqrt{\left(\omega_e\left(L_s I_d + \lambda_{pm}\right)\right)^2 + \left(\omega_e L_s I_q\right)^2} \tag{4.9}$$

and,

$$\hat{V}_o = G \cdot \frac{V_{dc}}{2} \tag{4.10}$$

Therefore, the voltage gain needed in BVFW control for operating the PMSM drive at any particular speed is given by:

$$G = \frac{2}{V_{dc}}\sqrt{\left(\omega_e\left(L_s I_d + \lambda_{pm}\right)\right)^2 + \left(\omega_e L_s I_q\right)^2} \tag{4.11}$$

4.3 CONTROL SCHEME FOR SPMSM DRIVES BASED ON ZSI

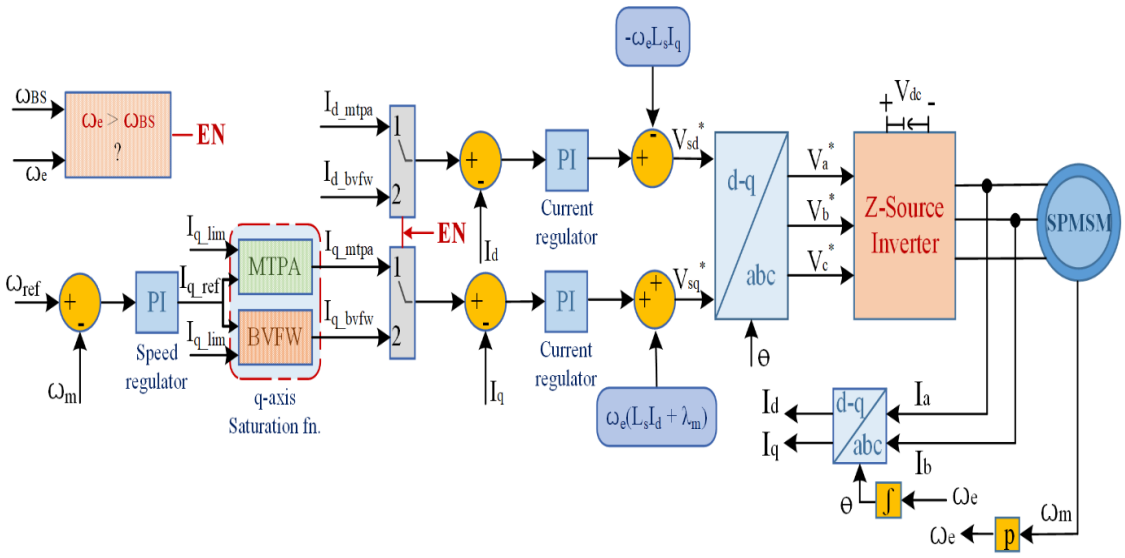

Fig.4.2: Control scheme for SPMSM drives based on ZSI.

Here, Fig. 4.2 shows the control scheme of SPMSM drive with boosted voltage flux-weakening control and maximum torque per ampere control. The operating zone of SPMSM drive is decided based on the decision whether the reference speed set is below or above the base speed value. In constant power zone, boosted voltage flux-weakening control is implemented while in constant torque zone MTPA control is implemented. The q-axis and d-axis currents generated by the respective MTPA and BVFW control strategies are limited by their saturation function, to ensure safe operation of motor by maintaining the thermal limits. The error produced by comparing reference speed and sensed speed in outer speed loop is fed to the speed regulator. The output of speed regulator sets the q-axis reference current, I_{q_ref}, which will be considered in the saturation function. The stator winding currents are transformed into the d-q frame utilizing rotor angle information obtained by integrating the electrical speed. After transformation these sensed currents are compared with their saturated current references, selected based on operating zone. The error produced is fed to the current regulators in

inner current control loops. Then to nullify the cross-coupling terms appearing in stator voltage equations, the outputs of current regulators are subjected to feed-forward compensation [48] and after that d-axis and q-axis reference voltages are obtained. These reference voltages are transformed into abc reference frame which finally be used as modulation signals in maximum boost control of a ZSI.

4.4 SIMULATION RESULTS

A wide speed range SPMSM drive is simulated to validate the boosted voltage flux-weakening algorithm with ZSI and its performance is compared with the conventional voltage and current constraints flux-weakening control without activating the control loops. The system ratings of the SPMSM drive with the ZSI are listed in the Table-4.1.

TABLE-4.1.

SYSTEM RATINGS

V_{DC}	485 V
Rated Speed	3000 RPM
Rated Torque	11 N-m
Pole Pair	3
Rated Current	6.9 A rms
Rated Voltage (l-l)	380 V rms
Peak Phase Voltage	310 V
Rated Power	3455 W
L_s	5.7 mH
R_s	0.965 Ω
λ_{pm}	0.2514 V-s
K_T	1.6 N-m/A rms
J	0.0011 Kg-m^2
$L_1 = L_2$	400 µH
$C_1 = C_2$	2200 µF
f_{SW}	5 KHz

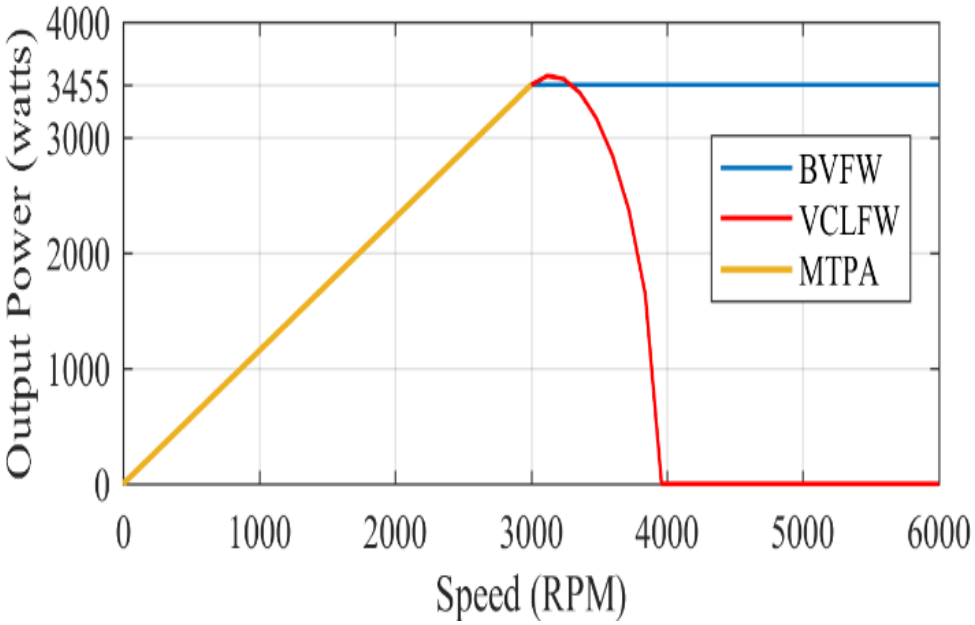

Fig.4.3: Output power vs speed trajectories.

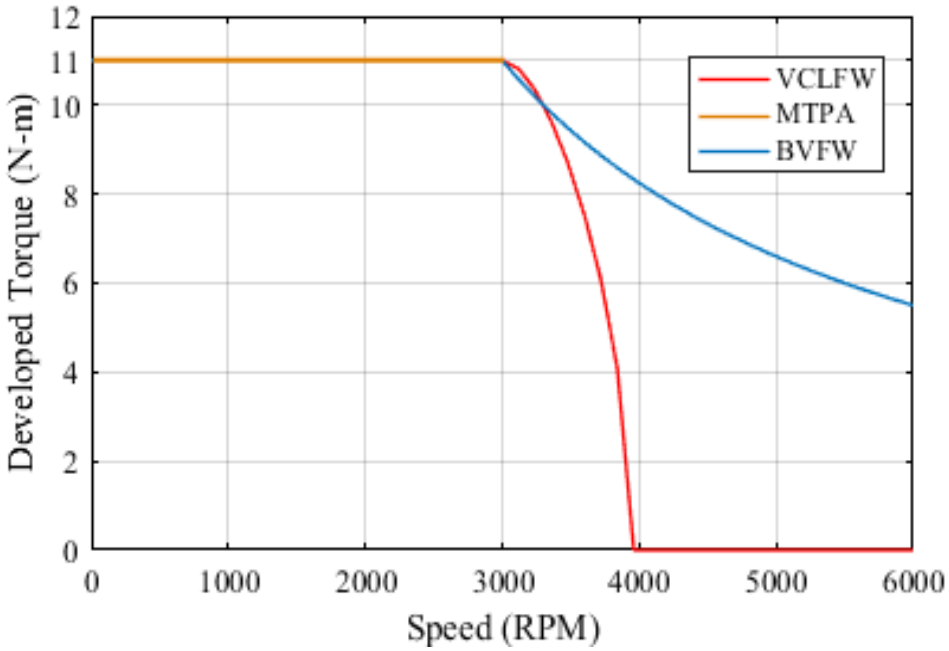

Fig.4.4: Developed torque vs speed trajectories.

From the output power-speed curve of SPMSM drive shown in fig. 4.3, it is clear that BVFW control can deliver constant power in flux-weakening zone which isn't possible in VCLFW control. From the developed torque-speed curve of SPMSM drive shown in fig. 4.4 shows, it is clear that BVFW control can deliver higher torque than the VCLFW control over a wide speed range without exceeding the current limit.

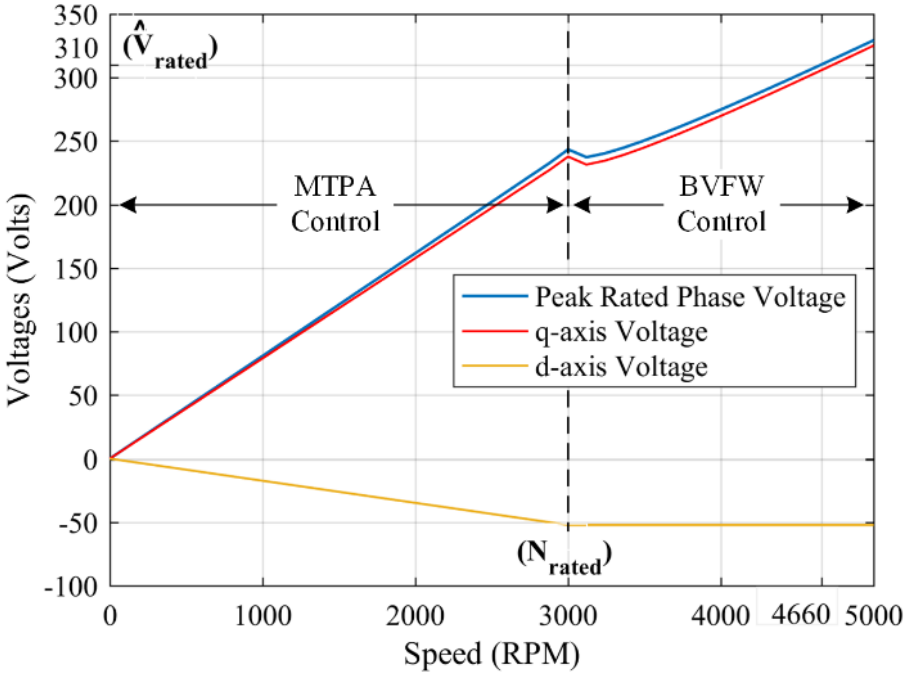

Fig.4.5: Voltage vs speed trajectories.

Fig. 4.5 shows the voltage trajectories of the SPMSM drive for the discussed MTPA and BVFW control strategies. The peak phase voltage rises linearly with the motor speed in constant torque zone while in the constant power zone it slightly decreases in the beginning and then again rises with the motor speed. It is observed that during the BVFW control, the peak phase voltage is significantly increased than the $\hat{V}_{s\_max}$ that a conventional inverter can output, i.e., $0.5V_{dc}$ (242.5 Volts) here. From the voltage vs speed trajectory, it is noticed that the rated peak phase voltage, which is 310 Volts, is attained at speed of 4560 rpm. Therefore, by implementing the BVFW control in constant power zone the speed range is extended by 52% which is 20% higher than which is obtained under VCLFW control.

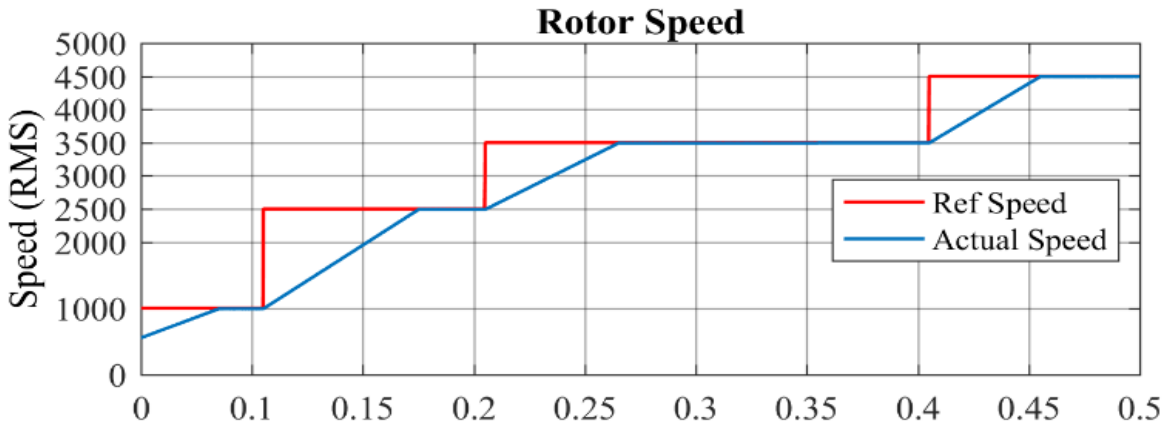

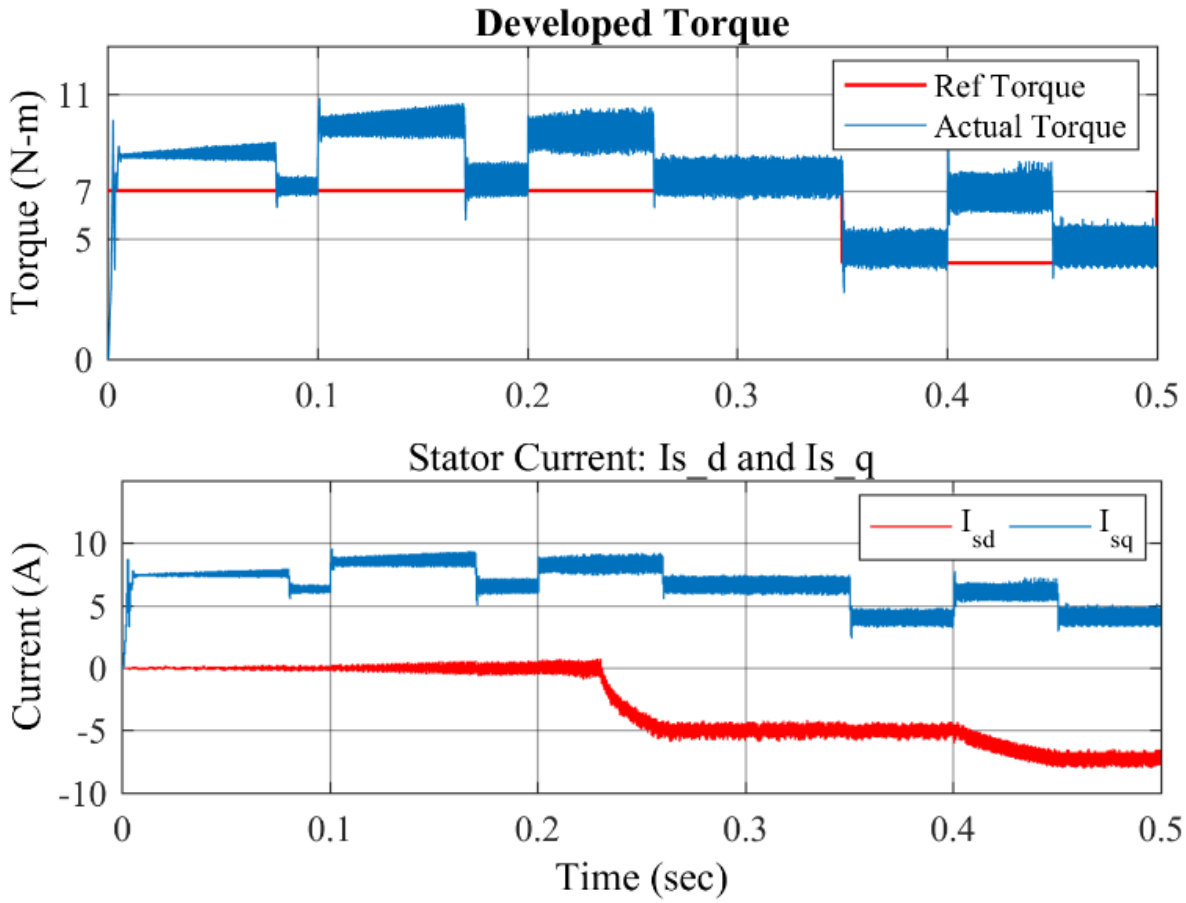

Fig.4.6: Dynamic performance under speed and load perturbations.

Fig. 4.6 shows the dynamic performance of SPMSM drive under speed and load perturbations. The drive effectively followed the reference speed up to 4500 rpm, which verifies the wide increase in constant power speed range, and delivers the demanded torque except during the speed perturbations and initial starting interval where increase in torque level indicates that drive is accelerating to attain steady state. In constant torque zone, d-axis current value is zero which is the optimal current for MTPA control of SPMSM while in constant torque zone, the d-axis current increases in the negative direction. The increase in d-axis is well within the maximum current limit and changes are in accordance to the expression derived in equation (4.7). The changes in q-axis current are in accordance to the variation in developed torque.

4.5 CONCLUSION

In this chapter, first in section 4.1 a brief introduction of the BVFW is presented then in section 4.2 an advanced boosted voltage flux-weakening algorithm based on ZSI is developed for SPMSM. In section 4.3 a wide speed range control scheme

for SPMSM drives is introduced in which MTPA control is implemented in constant torque zone while in constant power zone BVFW control is implemented. Further in section 4.4 the above-mentioned control scheme for SPMSM drives is simulated in MATLAB/Simulink environment under speed and load perturbations in order to validate the feasibility and merits of the ZSI based BVFW control. Additionally, in section 4.4 the performance of BVFW algorithm is compared with other flux-weakening algorithms and it is observed that BVFW control can maintain the output power constant during the flux-weakening operation and provides a substantial increase in operating speed range because of the boosted phase voltage which indicates that the drive's speed range during flux-weakening is not limited by the voltage constraints. At the same time, it can deliver higher torque over an extended constant power speed range without increasing the phase currents.

CHAPTER 5

SUMMARY AND CONCLUSION

5.1 SUMMARY

First, the literature review of PMSM, flux-weakening control techniques and ZSI is discussed in chapter 1 of this thesis. Then the problem related to the existence of large b-EMF values in flux-weakening zone is discussed. The concept of utilizing the voltage boosting abilities of ZSI aimed for achieving wide constant power speed range by overcoming the voltage constraint from drive becomes quite attractive because the commonly employed conventional 3-phase Inverter is basically a step-down converter.

Second, the mathematical modelling of PMSM is demonstrated in Chapter 2 of this thesis. In this chapter, the control algorithms for PMSM are also introduced including the MTPA and various flux-weakening strategies. Then a wide speed range SPMSM drive control scheme is discussed and realized in MATLAB/Simulink. in which MTPA and VCLFW control strategies are implemented for the low-speed and high-speed operations respectively.

Third, a brief introduction of the ZSI and its operating principle for different operating states is presented in chapter 3 of this thesis. Then the maximum boost control method for ZSI is introduced and the analytical expression for the voltage gain and peak inverter output voltage are obtained. With the aim to properly understand how capacitors and inductors are charging and discharging in the Z-impedance network, details of the active and shoot-through states of ZSI are analysed. In order to validate the voltage boosting abilities of ZSI and feasibility of control method, a ZSI model with the maximum boost control is simulated in MATLAB/Simulink.

Fourth, an advanced ZSI based flux-weakening strategy for SPMSM, namely, the boosted voltage flux-weakening is introduced in chapter 4 of this thesis. Then a wide speed range control scheme for SPMSM drives is discussed which includes the MTPA and BVFW control strategies for the constant torque zone and constant power zone respectively. Further, in order to validate the feasibility and merits of the ZSI based BVFW control the above-mentioned control scheme for SPMSM drives is simulated in

MATLAB/Simulink and the performance of BVFW algorithm is compared with other flux-weakening algorithms.

5.2 CONCLUSION

In this thesis, an advanced ZSI based boosted voltage flux-weakening strategy for SPMSM is discussed and simulated in MATLAB/Simulink environment. In high-speed operation, i.e., above base speed, overcoming the large b-EMF values of PMSM by utilising the voltage boosting abilities of ZSI is the main contribution of this thesis. The BVFW control can significantly extend the speed range of PMSM as compared to the conventional flux-weakening strategies. In order to validate the feasibility and merits of the ZSI based BVFW control a SPMSM drive is simulated in MATLAB/Simulink and the performance of BVFW algorithm is compared with other flux-weakening algorithms. From the simulation results it is observed that BVFW control can maintain the output power constant during the flux-weakening operation and provides a substantial increase in operating speed range because of the boosted phase voltage which indicates that the drive's speed range during flux-weakening is not limited by the voltage constraints. At the same time, it can deliver higher torque over an extended constant power speed range without increasing the phase currents.

REFERENCES

[1] Y. Zhang, L. Xu, M. Guven, S. Chi, and M. Illindala, “Experimental verification of deep field weakening operation of a 50-kW IPM machine by using single current regulator,” IEEE Trans. Ind. Appl., vol. 47, no. 1, pp. 128-133, 2011.

[2] J. F. Gieras and M. Wing, “Permanent magnet motor technology (Design and Application),” Marcel. Dekker, Inc., second edition, revised and expanded ed., 2002.

[3] S. Chi and L. Xu, “A special flux-weakening control scheme of PMSM - incorporating and adaptive to wide-range speed regulation,” Power Electronics and Motion Control Conference, vol. 2, pp. 1-6, 2006.

[4] H. Mahmoudi, A. Lagrioui, “Flux-weakening control of permanent magnet synchronous machines,” Journal of Theoretical and Applied Information Technology, ISSN: 1992-8645, 1992.

[5] L. Harnefors, K. Pietilainen, and L. Gertmar, “Torque-maximizing field-weakening control: design, analysis, and parameter selection,” IEEE Trans. Ind. Electron., vol. 48, no. 1, pp. 161-168, February 2001.

[6] N. Bianchi, S. Bolognani, and M. Zigliotto, “High-performance PM synchronous motor drive for an electrical scooter,” IEEE Trans. Ind. Appl., vol. 37, no. 5, pp. 1348-1355, Sep./Oct. 2001.

[7] G. Pellegrino, A. Vagati, and P. Guglielmi, “Design tradeoffs between constant power speed range, uncontrolled generator operation, and rated current of IPM motor drives,” IEEE Trans. Ind. Appl., vol. 47, no. 5, pp. 1995-2003, Sep./Oct. 2011.

[8] P. Pillay and R. Krisnan, “Modeling, simulation, and analysis of permanent magnet motor drives,” IEEE Trans. Ind. Appl., vol. IA-25, pp. 265–279, March/April 1989.

[9] G. Pellegrino, E. Armando, and P. Guglielmi, “Field oriented control of IPM drives for optimal constant power operation,” 2007 European Conference on Power Electronics and Applications, pp.1-10, Sept. 2007.

[10] J. Wai, T. M. Jahns, “A new control technique for achieving wide constant power speed operation with an interior PM alternator machine,” Industry Application Conference, vol. 2, pp. 807-814, 2001.

[11] K. W. Lee and S. B. Lee, “MTPA operating point tracking control scheme for vector controlled PMSM drives,” International Symposium on Power Electronics Electrical Drives Automation and Motion, pp. 24-28, June 2010.

[12] T. M. Jahns, “Flux-weakening regime operation of an interior permanent-magnet synchronous motor drive,” IEEE Trans. Ind. Appl., vol. IA-23, pp. 681-689, July/Aug. 1987.

[13] Q. Liu, “Analysis, design and control of permanent magnet synchronous motors for wide-speed operation,” Ph. D. dissertation, National University of Singapore, 2005.

[14] P. Zhang, “A novel design optimization of a fault-tolerant AC permanent magnet machine-drive system,” Ph. D. dissertation, Marquette University, Milwaukee, WI, Dec. 2013.

[15] G. Kohlrusz and D. Fodor, “Comparison of scalar and vector control strategies of induction motors,” Hungarian Journal of Industrial Chemistry, vol., 39, pp. 265-270, 2011.

[16] C. Capitan, “Torque control in field weakening mode,” Master Thesis, Aalborg University, Aalborg, Denmark, June 2009.

[17] H. Le-Huy, “Comparison of field-oriented control and direct torque control for induction motor drives,” Industry Application Conference, thirty fourth IAS annual meeting, vol. 2, pp. 1245-1252, Oct. 1999.

[18] M.F. Moussa, A. Helal, Y. Gaber, and H.A. Youssef, “Unity power factor control of permanent magnet motor drive system,” 12th International Middle-East Power System Conference, pp 360-367, March 2008.

[19] C. Mademlis, I. Kioskeridis, and N. Margaris, “Optimal efficiency control strategy for interior permanent-magnet synchronous motor drives,” IEEE Transaction on Energy Conversion, vol. 19, pp. 715-723, Dec. 2004.

[20] B. K. Bose, “Modern power electronics and AC drives,” Prentice Hall, Inc., 2002.

[21] W. L. Soong and N. Ertugrul, “Field-weakening performance of interior permanent magnet motors,” IEEE Trans. Ind. Appl., vol. 38, no. 5, pp. 1251-1258, Sep. / Oct. 2002.

[22] V. R. Jevremovic and D. P. Marcetic, “Closed-loop flux-weakening for permanent magnet synchronous motors,” 4th IET Conference on Power Electronics, Machines and Drives, pp. 717-721, April 2008.

[23] J. M. Kim and S. K. Sul, “Speed control of interior permanent magnet synchronous motor drive for the flux weakening operation,” IEEE Trans. Ind. Appl., vol. 33, no. 1, pp. 43-48, Jan. /Feb. 1997.

[24] S. Morimoto, M. Sanada and Y. Takeda, “Wide-speed operation of interior permanent magnet synchronous motors with high-performance current regulator,” IEEE Trans. Ind. Appl., vol. 30, no. 4, pp. 920-926, July/August 1994.

[25] J. R. Hendershot and T.J.E. Miller, “Design of brushless permanent-magnet machines,” Motor Design Books LLC, 2010.

[26] F. Giri, “AC electric motors control-advanced design techniques and applications,” A John Wiley & Sons, Ltd., 2013.

[27] N. Mohan, “Advanced electric drive,” MNPERE, 2001.

[28] B. K. Bose, “A high-performance inverter-fed drive system of an interior permanent magnet synchronous machine,” IEEE Trans. Ind. Appl., vol. 24, pp. 987- 997, Sept./Oct. 1991.

[29] H. Wen, W. Xiao, H. Li, X. Wen, “Analysis and Minimisation of DC Bus Voltage for Electric Vehicle Applications,” IET Electrical Systems in Transportation, vol. 2, pp. 68-76, June 2012.

[30] N. Mohan, T. M. Undeland, and W. P. Robbins, “Power Electronics,” John Wiley & Sons, Inc., third edition, 2003.

[31] F. Z. Peng, “Z-Source Inverter,” IEEE Trans. Ind. Appl., vol. 39, no. 2, pp. 504-510, March/April 2003.

[32] J. Anderson and F. Z. Peng, “Four Quasi-Z-Source Inverter,” Power Electronics Specialist Conference 2008, pp. 2743-2749, June 2008.

[33] K. Holland and F. Z. Peng, “Control Strategy for Fuel Cell Vehicle Traction Drive Systems Using the Z-Source Inverter,” Vehicle Power and Propulsion, 2005 IEEE Conference, pp. 639-644, Sept. 2005.

[34] Q. Lei, S. Yang, F. Z. Peng, and R. Inoshita, “Application of Current-fed QuasiZ-Source Inverter for Traction Drive of Hybrid Electric Vehicles,” Vehicle Power and Propulsion Conference, pp. 754-760, Sept. 2009.

[35] F. Z. Peng, A. Joseph, J. Wang, M. Shen, L. Chen, Z. Pan, E. O. Rivera, and Y. Huang, “Z-Source Inverter for Motor Drives,” IEEE Trans. on Power Electron, vol. 20, no. 4, pp. 857-863, July 2005.

[36] F. Z. Peng, X. Yuan, X. Fang and Z. Qian, “Z-Source Inverter for Adjustable Speed Drives,” IEEE Power Electronics Letters, vol. 1 no. 2, pp. 33-35, June 2003.

[37] B. Ge, Q. Lei, W. Qian and F. Z. Peng, “A family of Z-source matrix converters,” IEEE Transactions on Industrial Electronics, vol. 59, no. 1, pp.35-46, Jan. 2003.

[38] F. Gao, P. C. Loh, F. Blaabjerg and D. M. Vilathgamuwa, “Performance evaluation of three level Z-source inverters under semiconductor-failure conditions,” IEEE Trans. Ind. Appl., vol. 45, no. 3, pp. 971-981, May/ Jun. 2009.

[39] M. Zhu, K. Yu, and F.L. Luo, “Switched inductor Z-source inverter”, IEEE Trans. on Power Electron., vol. 25, no. 8, pp. 2150-2158, Aug. 2010.

[40] Y. Tang, S. Xie, C. Zhang, and Z. Xu, “Improved Z-source inverter with reduced Z-source capacitor voltage stress and soft-start capability”, IEEE Trans. on Power Electron., vol. 24, no. 2, pp. 409-415, Feb. 2009.

[41] M. Shen, J. Wang, A. Joseph, F.Z. Peng, L.M. Tolbert, and D.J. Adams, “Maximum constant boost control of the Z-source inverter,” IEEE Trans. Ind. Appl., vol. 42, no. 3, pp. 770-777, May/Jun. 2006.

[42] F.Z. Peng, M. Shen, and Z. Qian, “Maximum boost control of the Z-source inverter”, IEEE Trans. on Power Electron., vol. 20, no. 4, pp. 833-838, Jul. 2005.

[43] Q. Lei, D. Cao, and F. Z. Peng, “Novel loss and harmonic minimized vector modulation for a current-fed quasi-Z-source inverter in HEV motor drive application,” IEEE Trans. on Power Electron., vol. 29, no. 3, pp. 1344-1357, Mar. 2014.

[44] A. M. El-Refaie and T. M. Jahns, “Optimal flux weakening in surface PM machines using fractional-slot concentrated windings,” IEEE Trans. Ind. Appl., vol. 41, no. 3, pp. 790-800, May/Jun. 2005.

[45] A. Tessarolo, M. Mezzarobba, and R. Menis, “A novel interior permanent magnet motor design with a self-activated flux-weakening device for automotive applications,” 2012 International Conference on Electrical Machines, pp. 2603-2609, Sept. 2012.

[46] M. E. Haque, L. Zhong, and M. F. Rahman, “Improved trajectory control for an interior permanent magnet synchronous motor drive with extended operating limit,” Journal of Electrical & Electronics Engineering, Australia, vol. 22, no. 1, 2003.

[47] Z. Mihailovic, “Modeling and control design of VSI-fed PMSM drive system with active load,” Master Thesis, Virginia Polytechnic Institute and State University, Blacksburg, Virginia, Jun. 1998.

[48] K. Lee and J.-I. Ha, “Dynamic Decoupling Control Method for PMSM Drive with Cross-Coupling Inductances,” in 2017 IEEE Applied Power Electronics Conference and Exposition (APEC), Tampa, FL, 2017.

[49] J. Wang, J. Wu, C. Gan and Q. Sun, “Comparative study of flux-weakening control methods for PMSM drive over wide speed range,” in 2016 19th International Conference on Electrical Machines and Systems (ICEMS), Chiba, Japan, 2016.

[50] M. Shen, J. Wang, A. Joseph, F. J. Peng, L. M. Tolbert and J. A. D., “Constant boost control of the Z-source inverter to minimize current ripple and voltage stress,” IEEE Transactions on Industry Applications, vol. 42, no. 3, pp. 770-778, May-Jun 2006.

LIST OF PUBLICATIONS

[1] Abhishek Dalal, Mini Sreejeth, “Wide Speed Range Control of PMSM Based on MTPA and Flux-Weakening Control” in 4th International Conference on Power, Instrumentation, Control and Computing (PICC2023). **(Accepted and Presented)**

[2] Abhishek Dalal, Mini Sreejeth, “Z-Source Inverter Based Boosted Voltage Flux-Weakening Control of SPMSM” in 2023 3rd Asian Conference on Innovation in Technology (ASIANCON). **(Communicated)**